Technology

Molecular Cell

Efficient and Accurate Quantitative Profiling of Alternative Splicing Patterns of Any Complexity on a Laptop

Graphical Abstract

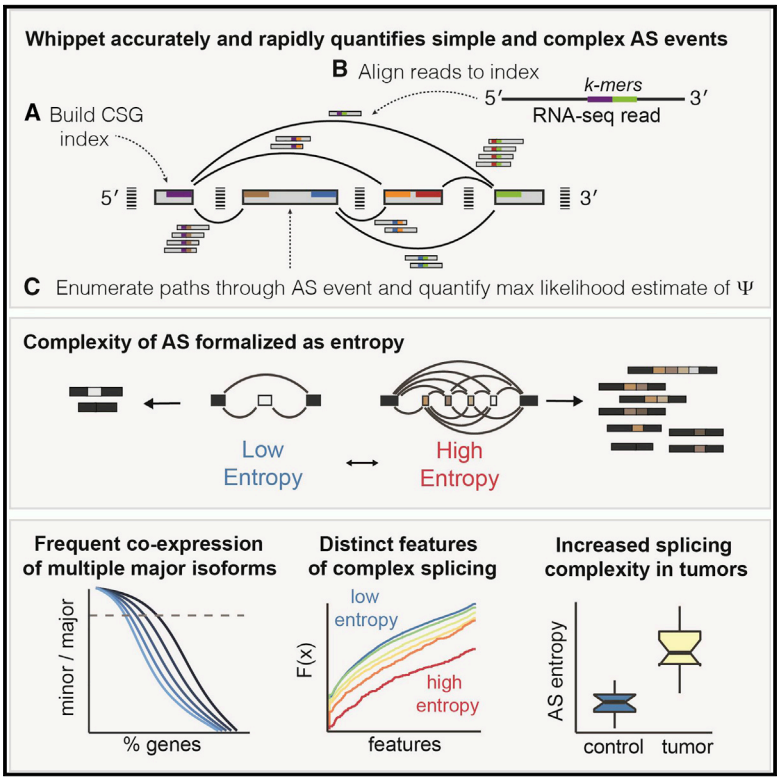

Highlights

- Whippet, a new method for the rapid and accurate profiling of alternative splicing
- Whippet reliably detects and quantifies complex alternative splicing events
- Approximately one-third of human genes simultaneously express multiple major isoforms
- Complex splicing events are conserved, tissue regulated, and more prevalent in cancer

Authors

Timothy Sterne-Weiler, Robert J. Weatheritt, Andrew J. Best, Kevin C.H. Ha, Benjamin J. Blencowe

Correspondence

tim.sterne.weiler@utoronto.ca (T.S.-W.), b.blencowe@utoronto.ca (B.J.B.)

In Brief

Sterne-Weiler et al. describe Whippet, a method for the rapid and accurate quantitative profiling of alternative splicing from RNA-seq data. Whippet is particularly effective in the analysis of complex alternative splicing events, revealing that they impact up to 40% of human genes, are often conserved, and are elevated in cancer.

Sterne-Weiler et al., 2018, Molecular Cell 72, 187–200
October 4, 2018
https://doi.org/10.1016/j.molcel.2018.08.018

CellPress

Molecular Cell
Technology

Efficient and Accurate Quantitative Profiling of Alternative Splicing Patterns of Any Complexity on a Laptop

Timothy Sterne-Weiler,[1,5,*] Robert J. Weatheritt,[1,2,4,5] Andrew J. Best,[1] Kevin C.H. Ha,[1,3] and Benjamin J. Blencowe[1,3,6,*]
[1]Donnelly Centre, University of Toronto, Toronto M5S 3E1, Canada
[2]MRC Laboratory of Molecular Biology, Francis Crick Avenue, Cambridge CB2 0QH, UK
[3]Department of Molecular Genetics, University of Toronto, Toronto M5S 3E1, Canada
[4]EMBL Australia, Garvan Institute of Medical Research, 384 Victoria Street, Darlinghurst, New South Wales 2010, Australia
[5]These authors contributed equally
[6]Lead Contact
*Correspondence: tim.sterne.weiler@utoronto.ca (T.S.-W.), b.blencowe@utoronto.ca (B.J.B.)
https://doi.org/10.1016/j.molcel.2018.08.018

SUMMARY

Alternative splicing (AS) is a widespread process underlying the generation of transcriptomic and proteomic diversity and is frequently misregulated in human disease. Accordingly, an important goal of biomedical research is the development of tools capable of comprehensively, accurately, and efficiently profiling AS. Here, we describe Whippet, an easy-to-use RNA-seq analysis method that rapidly—with hardware requirements compatible with a laptop—models and quantifies AS events of any complexity without loss of accuracy. Using an entropic measure of splicing complexity, Whippet reveals that one-third of human protein coding genes produce transcripts with complex AS events involving co-expression of two or more principal splice isoforms. We observe that high-entropy AS events are more prevalent in tumor relative to matched normal tissues and correlate with increased expression of proto-oncogenic splicing factors. Whippet thus affords the rapid and accurate analysis of AS events of any complexity, and as such will facilitate future biomedical research.

INTRODUCTION

High-throughput RNA sequencing (RNA-seq) technologies are producing vast repositories of transcriptome profiling data at an ever-expanding pace (Silvester et al., 2018). This explosion in data has enabled genome-wide investigations of the role of alternative splicing (AS) in gene regulation and its dysregulation in human diseases and disorders. Initial investigations using RNA-seq data revealed that ~95% of human multi-exon gene transcripts undergo AS (Pan et al., 2008; Wang et al., 2008). These and more recent studies analyzing ribosome-engaged transcripts and quantitative mass spectrometry data suggest that AS is a major process underlying the generation of transcriptomic and proteomic complexity (Floor and Doudna, 2016; Liu et al., 2017; Sterne-Weiler et al., 2013; Weatheritt et al., 2016; reviewed in Blencowe, 2017). Furthermore, numerous AS events belonging to co-regulated and evolutionarily conserved exon networks have been shown to provide critical functions in diverse processes (Baralle and Giudice, 2017; Tapial et al., 2017).

A major challenge confronting genome-wide investigations of AS is that existing methods for analyzing RNA-seq data require extensive computational resources and expertise. For example, widely employed tools involve alignment of reads to a transcriptome or reference genome, followed by quantification by downstream methods that estimate percent spliced in (PSI, Ψ) values for each AS event, such as cassette exons, alternative 5′ and 3′ splice sites, and retained introns. These steps can be time consuming and typically present a bottleneck when analyzing large datasets.

Recent developments in transcript expression quantification have circumvented traditional alignment steps by extracting k-mers (i.e., all possible sequences of length k) from reads to identify possible transcripts of origin. Such methods can decrease processing times by 10- to 100-fold (Bray et al., 2016; Patro et al., 2017). However, their accuracy relies on whole "transcript-level" annotation models (i.e., models that record the precise location of intron and exon boundaries, and spliced junctions, for all transcripts), which are incomplete for the majority of species, and inconsistent among even the best-annotated species. The lack of complete annotation models can thus confound the accurate detection and quantification of AS events when using transcript-level methods. More widely used methods for RNA-seq analysis, focusing on the local detection and quantification of AS events, are referred to below as "event-level" approaches (Figure S1A; Katz et al., 2010; Tapial et al., 2017; Wang et al., 2017). These methods can achieve considerable accuracy for simple AS events (Vaquero-Garcia et al., 2016), yet existing tools are computationally inefficient in comparison with transcript-level methods, and most utilize predetermined simple binary models (i.e., a single alternative exon surrounded by two constitutive exons),

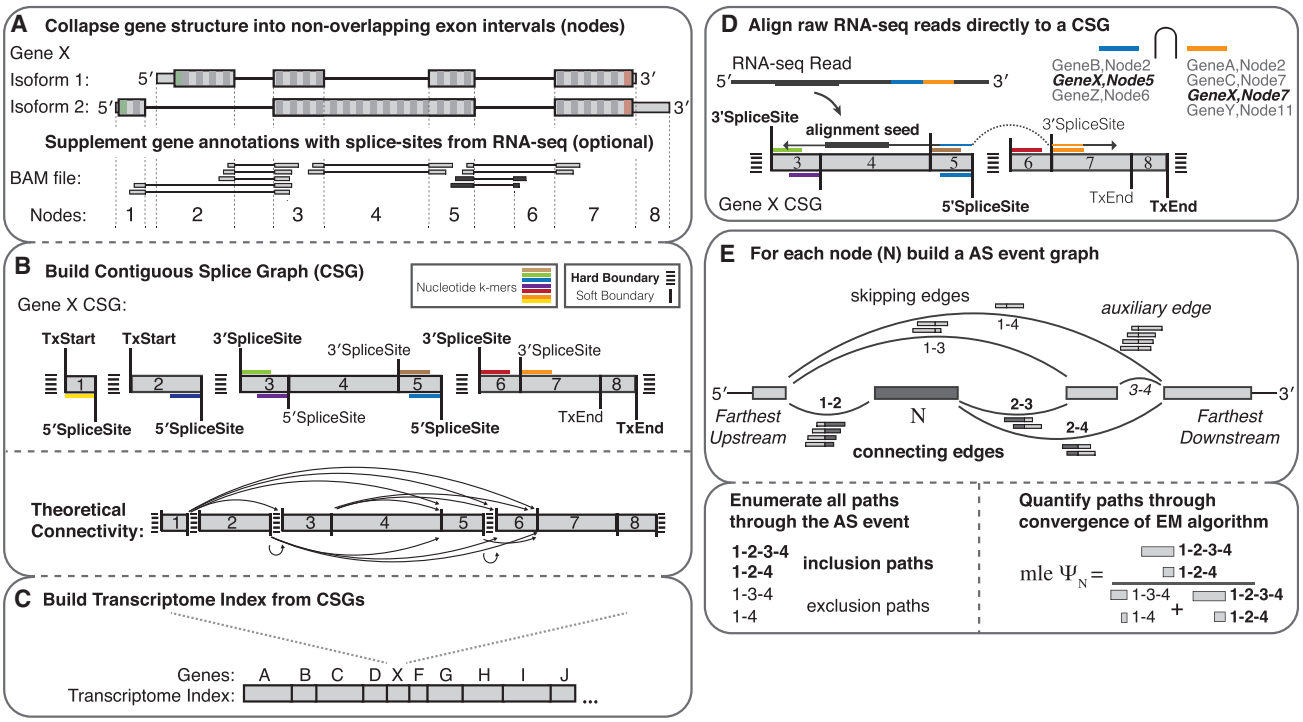

Figure 1. Overview of Whippet

(A) Example gene model with two alternative isoforms and Whippet's node assignments as indicated by number and separated by dashed lines. Gene models can be supplemented beyond standard annotation sets with new splice sites and novel exons mined using *de novo* spliced read aligners (see also Figure S1E).

(B) The contiguous splice graph (CSG) for the gene model in (A). Each CSG node has two boundaries: an incoming (left side of node, label pointing upward) and outgoing (right side of node, pointing downward), and these have "soft" or "hard" alignment extension properties (see D). Boundary types are designated as hard or soft depending on whether or not a genomic sequence separates two neighboring nodes, respectively. All 5′ SpliceSite and 3′ SpliceSite boundaries have k-mer indices (colored lines) that are used for spliced read alignment (middle top). Lines with arrows indicate potential connectivity (edges) between nodes (middle bottom).

(C) A single transcriptome full-text index in minute space (FM-Index) is built from concatenated CSG sequences, with solid lines indicating separation between each CSG (bottom).

(D) Diagram of CSG alignment, which is seeded from a raw RNA-seq read and then extended in both directions. Alignments can extend through soft but not hard boundaries. The two read k-mers flanking a spliced node boundary are used to return the set of compatible nodes for spliced junction extension (see STAR Methods for CSG alignment rules).

(E) Example Whippet AS event (top) for a node *N*, defined as the full set of spliced edges aligned (in an RNA-seq dataset) between the nodes farthest upstream or downstream for connecting (bolded labels) or skipping edges (regular labels). To determine percent spliced in (Ψ) of some node *N*, all paths through the AS event are enumerated (bottom left) and quantified through convergence of the expectation-maximization (EM) algorithm (bottom right) (see STAR Methods). Paths including the node *N* are bolded. mle, maximum likelihood estimate.

making them poorly suited for the analysis of complex AS patterns.

In light of these challenges, an important goal for understanding how transcriptomes shape biological processes is to develop methods capable of accurately analyzing simple and complex AS patterns with high efficiency. To address these challenges, we have developed Whippet, an easy-to-use, event-level software tool for the accurate and efficient detection and quantification of AS events of any complexity. Whippet has computational requirements compatible with a laptop computer and is capable of analyzing reads streamed from web-accessible data files by entering a file accession number. Another feature of Whippet is that it uses an entropic measure of AS to facilitate the accurate profiling of AS. We demonstrate the utility of Whippet in the discovery of previously uncharacterized AS complexity in vertebrate transcriptomes associated with the regulation of tandem domains and other protein sequence features, as well as a remarkable increase in AS complexity in cancer transcriptomes.

DESIGN

Efficient Quantification of Alternative Splicing Using Whippet

Whippet models transcriptome structure by building "contiguous splice graphs" (CSGs). These are directed graphs whose nodes are non-overlapping exonic sequences, and edges (i.e., connections between nodes) represent splice junctions or adjacent exonic regions (Figures 1A and 1B). Splice graphs allow single isoforms to be represented as paths through nodes in the graph (Heber et al., 2002; Trapnell et al., 2010; Vaquero-Garcia et al., 2016). Whippet's CSGs extend the concept of splice graphs to a lightweight data structure that indexes the

transcriptome for fast and modular alignment of raw RNA-seq reads across splice junctions (Figures 1B and 1C). To facilitate indexing, Whippet defines incoming and outgoing boundary types (e.g., 5′ or 3′ splice sites or transcription start or end sites; refer to Figure 1B legend for details) that specify the theoretical connectivity through the CSG for each node (Figures 1B and S1B). For each 5′ or 3′ splice site boundary, Whippet's CSG index records an upstream or downstream k-mer, respectively, so as to enable efficient spliced read alignment across all possible splice junctions; this includes junctions that do not occur within annotated transcripts but which combine annotated donor or acceptor splice sites (Figures 1B–1D, S1C, and S1D; see STAR Methods for details). For example, Whippet's CSG index for the human genome hg19 build can represent AS events from >1.3 million exon-exon junctions in >2.3 billion theoretically possible isoform paths, whereas only ~100,000 of these paths are found in GENCODE v25 TSL1 annotated transcripts.

After alignment, a Whippet AS event is defined as the collective set of a node's skipping or connecting edges (e.g., edge 1-3 skips node 2, and edges 1-2 and 2-3 connect to node 2 in Figure 1E; see STAR Methods). When enumerating paths through a node's AS event, it is possible that multiple paths share common (i.e., ambiguous) edges (e.g., edges 1-2 and 3-4 are shared among multiple paths in Figure 1E). Therefore, to accurately quantify all AS events, the proportional abundance of each path is determined using maximum likelihood estimation by the expectation-maximization (EM) algorithm (see STAR Methods). The percent spliced in (PSI, Ψ; range 0.0 to 1.0) value of a node is then calculated as the sum of the proportional abundance of the paths containing the node (Figure 1E).

RESULTS

Whippet Facilitates Accurate Analysis of Alternative Splicing

To assess Whippet's accuracy, we compared its Ψ values with those measured from RT-PCR data and commonly used RNA-seq event-level analysis tools (Irimia et al., 2014; Katz et al., 2010; Wang et al., 2017; Vaquero-Garcia et al., 2016)—which quantify Ψ using reads that directly map to an AS event—as well as transcript-level tools (Trincado et al., 2018), which estimate Ψ based on reads mapping across entire transcripts (see Methods S1 and Figures S2A–S2G for details of mapping benchmarking). RT-PCR-derived and RNA-seq-derived Ψ values were both from adult mouse liver and cerebellum, as well as from stimulated and unstimulated human Jurkat T cell line samples (Vaquero-Garcia et al., 2016). Notably, Whippet and the other event-level tools display ~2.5-fold lower median error profiles compared to transcript-level methods, including SUPPA2 (Trincado et al., 2018) and Whippet_TPM, an approach developed in the present study to afford direct comparisons of transcript-level Ψ estimates that maintain Whippet's node definitions (Figures 2A, S2H, S3A, and S3B; Table S1; STAR Methods).

Benchmarking against RT-PCR Ψ values, while informative, is limited by the relatively small sample set (n = 162), the types of the events assessed, and possible intrinsic technical biases introduced by PCR. To address this, we assessed the accuracy of Whippet relative to other tools when comparing their Ψ values against synthetic (i.e., "ground truth") Ψ values simulated from RNA-seq data obtained from a reference transcriptome annotation (GENCODE v25 TSL1 for hg19; STAR Methods).

In contrast to results from benchmarking against RT-PCR data, we find that transcript-level methods perform with similar accuracy to event-level approaches, including Whippet, when using simulated RNA-seq data (compare Figures 2A and 2B). This discrepancy is likely due to the artificial nature of the simulation, where the exact transcript-annotations used to generate the reads are provided to the quantification software. In the analysis of RNA-seq data from biological samples, the quantification software will likely be challenged by discrepancies between the annotation model and the set of true transcripts present in the sample (e.g., Figure 2C shows that a large percentage of alternative splice junctions in vertebrate species are not annotated in Ensembl). To investigate such effects, we simulated RNA-seq reads with ground-truth Ψ values using one annotation set (RefSeq Release 84 for hg19) and created an index database for each quantification program using another annotation set (GENCODE v25 TSL1 for hg19). Notably, in this comparison (and the inverse comparison in Figure S3C) there is a 2- to 2.5-fold increase in error rate for estimating Ψ values using transcript-level methods, but minimal change in error rate for any of the event-level tools, including Whippet (Figures 2B and S3D). We conclude that differences in transcript reference annotations can confound estimates for Ψ values when using transcript-level methods, whereas event-based methods are largely insensitive to this issue.

The analyses so far used widely employed transcript annotations from human and mouse, which are among the most complete for any species. To assess Whippet's performance when analyzing species with less extensively annotated transcripts, we applied it to RNA-seq data (Brawand et al., 2011) from five of the same tissues from gorilla, chimp, opossum, and chicken as well as from mouse and human. While ~12% of alternative exon-exon junctions aligned by Whippet in human and mouse are unannotated, the percentage of unannotated AS junctions is in the range of 40%–80% in the other species (Figure 2C). These observations further indicate that transcript-level tools, and event-level tools reliant on annotated AS events, fail to detect a considerable amount of unannotated transcript diversity in vertebrates. In contrast, Whippet can detect and accurately quantify AS events involving numerous unannotated splice junctions represented by pairings of combinations of splice sites from its CSG indices (see also below).

The benchmarks described so far focus on "simple" AS events, such as single-cassette alternative exons flanked by pre-defined constitutive exons that have binary splicing outcomes. However, many AS events involve splice sites that are variably paired with two or more other sites. Whippet provides output metrics designed to quantify such AS complexity in two related ways. First, it classifies AS events into discrete bins of complexity based on the number of enumerated paths from the event (i.e., $n = \lceil log_2(paths) \rceil$ such that K(n) can produce at most 2^n spliced outcomes for K1, …, K6; Figure 2D). Second, it calculates a Ψ-dependent measure of AS complexity using Shannon's entropy (i.e., entropy = $-\Sigma_i \Psi_i \, log_2 \, \Psi_i$ such that the maximum entropy for an event in K(n) is n; Figures 2E, S4A,

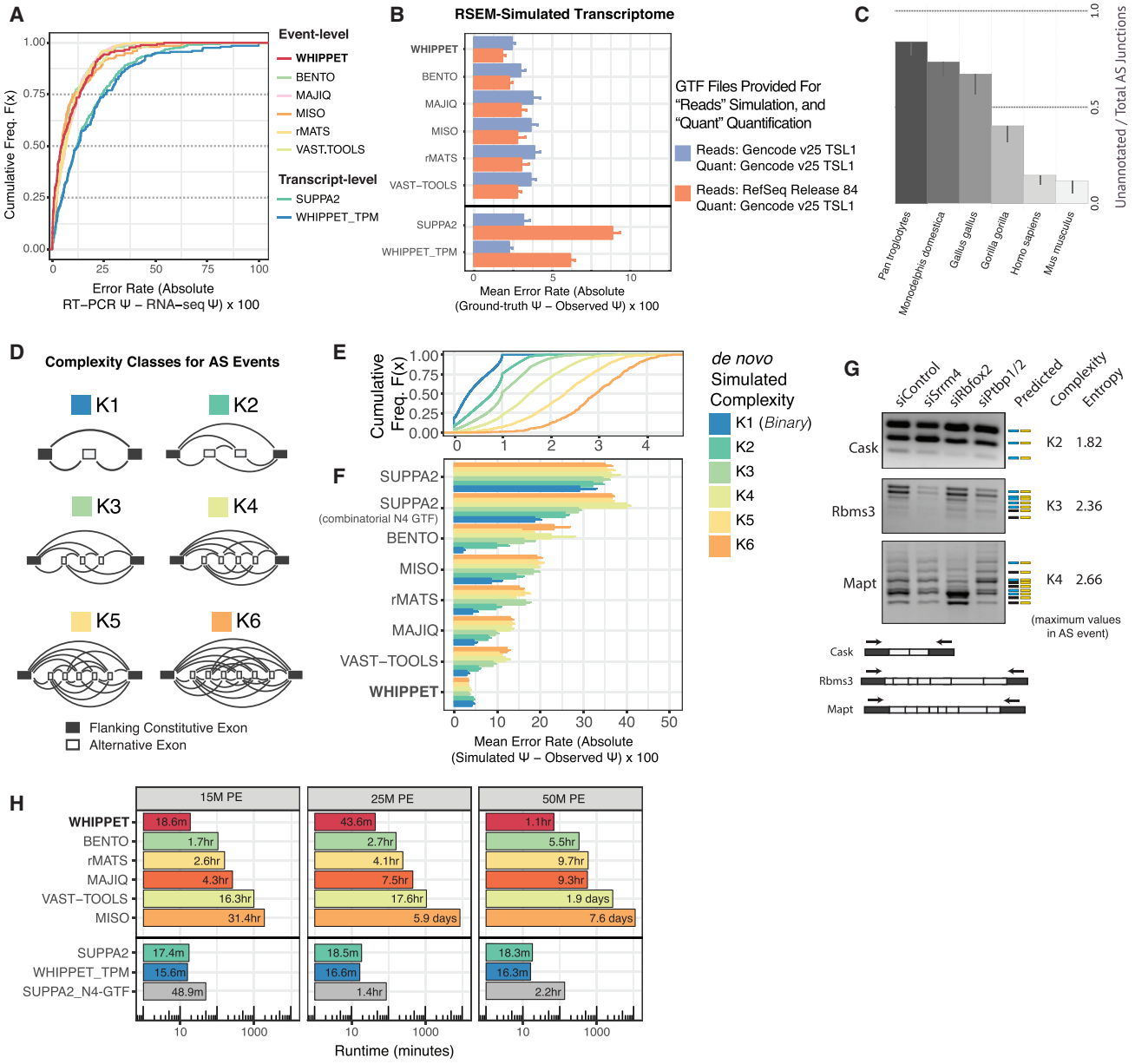

Figure 2. Whippet Benchmarking against Event-Level and Transcript-Level Approaches

(A) Cumulative distribution plot comparing percent spliced in (Ψ) values from RT-PCR data with Ψ values quantified from RNA-seq data. RT-PCR and RNA-seq data were generated from the same samples of mouse liver and cerebellum as well as from stimulated and unstimulated human Jurkat T cell line samples (Vaquero-Garcia et al., 2016). By default, all benchmarked programs were supplied with the full Ensembl GRCh37.73 annotation file unless indicated otherwise (see Table S4). Cumulative distribution plots describe the proportion of data (y axis) less than or equal to a specified value (x axis). Dotted y axis lines mark the lower quartile, median, and upper quartile (25%, 50%, and 75%) values, respectively. Cumulative Freq F(x), cumulative distribution function.

(B) Bar plots showing the absolute error rate of quantification algorithm Ψ values compared to simulated ground truth (i.e., known) Ψ values. Error bars represent the standard error of the mean. RSEM, RNA-seq by expectation maximization (Li and Dewey, 2011).

(C) Bar graph displaying the fraction of unannotated junctions (with two or more supporting reads) as a total of all junctions identified by Whippet across six vertebrate species (Brawand et al., 2011). "Error bars" represent the y axis value range for a cumulative number of tissues, one (lower bound of the error bar) to five (height of the bar). Source of annotation (left to right): panTro4 Ensembl; monDom5 Ensembl; galGal4 Ensembl; gorGor3 Ensembl; hg19 GENCODE v27 tsl1; mm10 GENCODE VM11 Basic.

(D) Formalization of AS complexity into discrete categories K(n). n, theoretical number of alternative nodes; K(n) = 2^n, spliced outcomes for a given AS event. Schematics of K(n) show constitutive exons (dark gray) and alternative exons (light gray) with curved lines representing all potential exon-exon junctions.

(E) Cumulative distribution of entropy scores (i.e., entropy = $-\Sigma_i\, \Psi_i\, log_2\, \Psi_i$) detected by Whippet for simulated AS events of different categories of complexity according to (D). See Figure 2A legend for a description of cumulative distribution plots.

(legend continued on next page)

and S4B). This entropic measure conveniently formalizes the total number of possible outcomes for an event and the degree of their proportional contribution to the transcriptome in a read-depth- and read-length-independent manner (Figures S4C and S4D)

To assess whether Whippet accurately quantifies AS events with increasing degrees of complexity and entropy, we simulated RNA-seq datasets and corresponding Ψ values for events in the formalized categories (K1, …, K6) of increasing complexity and distributed entropy (Figures 2D, 2E, and S4E). In contrast to other methods tested, the accuracy of Whippet-derived estimates for Ψ does not decrease as the complexity and entropy of the simulated AS events increases. This difference in performance is because Whippet has the unique feature among the event-level approaches tested of employing the EM algorithm to assign reads that are ambiguously shared between multiple paths through high-entropy AS events. This capability translates as a ~2-3 fold greater accuracy for Whippet in the quantification of K2-K6 events than for other tested methods (Figures 2E, 2F, and S4F).

To further assess Whippet's performance relative to other methods, we next investigated whether transcript-level methods potentially achieve comparable accuracy when provided with a predefined annotation set that comprehensively represents complex events. To test this, we built a transcript annotation set from combinatorial Whippet graph paths (N4 annotation file, STAR Methods). While this annotation set allows SUPPA2 to detect unannotated AS events, its error rate in estimating Ψ values is still 4-fold higher than Whippet's (Figures 2F, S4E, and S4F).

To experimentally validate Whippet-derived predictions of high AS-event entropy, RNA-seq data (Raj et al., 2014) from mouse neuroblastoma (N2a) cells were analyzed and 10 events with different predicted degrees of entropy and complexity involving tandem arrays of alternative exons were tested by RT-PCR (STAR Methods). Notably, 56/61 (91.8%) of the amplified spliced products were predicted by Whippet, whereas five (8.2%) of the expected isoforms were not detected. Of the detected products, 32 (52.5%) are consistent with annotated isoforms and 24 (39.3%) correspond to novel isoforms (Figures 2G and S5A). Collectively, these data demonstrate that Whippet is an accurate method for the analysis of both simple and complex AS events.

Efficiency of Whippet

To assess Whippet's efficiency, we benchmarked speed and memory usage relative to published AS quantification methods. When analyzing several paired-end RNA-seq datasets from HeLa cells with increasing read depth (~15 M, ~25 M, and ~50 M), Whippet quantifies AS from a raw paired-end 25 M RNA-seq read dataset in 43 minutes while using less than 1.5 GB of memory on a typical cluster node with a single core (Dual-Core AMD Opteron(tm) Processor 8218, 2.5 GHz, 60GB RAM, 1,024KB cache). This represents a considerable increase in performance over other tested event-level tools, and is of comparable performance to transcript-level methods (Figures 2H, S5B, and S5C; Table S2). For example, MISO, the most highly cited event-level tool, in combination with the read aligner STAR, took days and used 30 GB of memory to analyze the same data (Figures 2H and S5C), whereas the fastest transcript-level methods took approximately 20 minutes. It is important to note that when provided with annotation sets for complex AS events (e.g., N4 annotation file) the runtime and memory usage of transcript-level methods were greater than that of Whippet (Figures 2H and S5C). Moreover, on a personal laptop with a solid-state hard drive (Macbook Pro 3.1 GHz Intel i7), Whippet quantified the ~25 M dataset in 15 minutes using downloaded data files and in 31 minutes when streaming data from the internet after inputting the SRA identifier. The considerably longer time taken to analyze the same data by MISO and some of the other event-level tools may be influenced by the hardware used to run these programs. The unique features of Whippet thus obviate the use of high-performance computational clusters for the quantitative profiling of AS using RNA-seq data.

Taken together with the assessment of accuracy, the results indicate that Whippet offers advantages over other methods in terms of its capacity to reliably and efficiently detect and quantify AS events.

Detection of High-Entropy, Tissue-Regulated AS Events

Because previously described tools were not designed for the formalized quantitative profiling of AS complexity, we used Whippet to investigate the prevalence and possible biological relevance of high-complexity AS events in mammalian transcriptomes. To this end, we applied Whippet to an analysis of 60 diverse human and mouse tissue RNA-seq datasets (Table S3; Figures 3A and S6A). Remarkably, of more than 13,000 analyzed human protein coding genes, 42.68% harbor an AS event predicted to have an entropy >1.0 (i.e., two or more expressed isoforms) in at least one tissue (Figure S6B; see STAR Methods). Moreover, 4,101 (30.1%) of these genes co-express at least two major isoforms at similar levels in one or more of the same tissue (Figures 3B and S6C; STAR Methods). The majority (~20%) of events are predicted to undergo substantial tissue-dependent changes in splicing entropy (Figure 3C) without concurrent changes in expression of the corresponding genes

(F) Comparison of the ability of different RNA-seq analysis methods to detect AS events from simulated reads (STAR Methods) of complexity as defined in (D). Bar plots show the absolute mean error rate as a function of increasing complexity of AS. Error bars indicate standard error. Ψ, percent spliced in.

(G) RT-PCR analysis confirms the numerous splice isoforms in N2a cells for AS events of increasing levels of complexity and matching Whippet predictions for the maximal complexity and entropy (far right). Boxes to right of gels display UCSC (left, blue) and Whippet (right, yellow) in silico predictions based on expected primer amplification products (STAR Methods). Colored boxes (blue and yellow), correct predictions; black boxes, possible missed predictions. Diagrams below show exon structures of analyzed AS events with approximate positions of RT-PCR primers. Predicted constitutive and alternative exons are in dark and light gray, respectively (see legend in D).

(H) Comparison of the log-scaled "core" time requirements (i.e., taking into account time spent using multiple cores) for running Whippet relative to published methods for RNA-seq splicing quantification when analyzing 15 M, 25 M, or 50 M paired-end RNA-seq read datasets (see STAR Methods and Table S3).

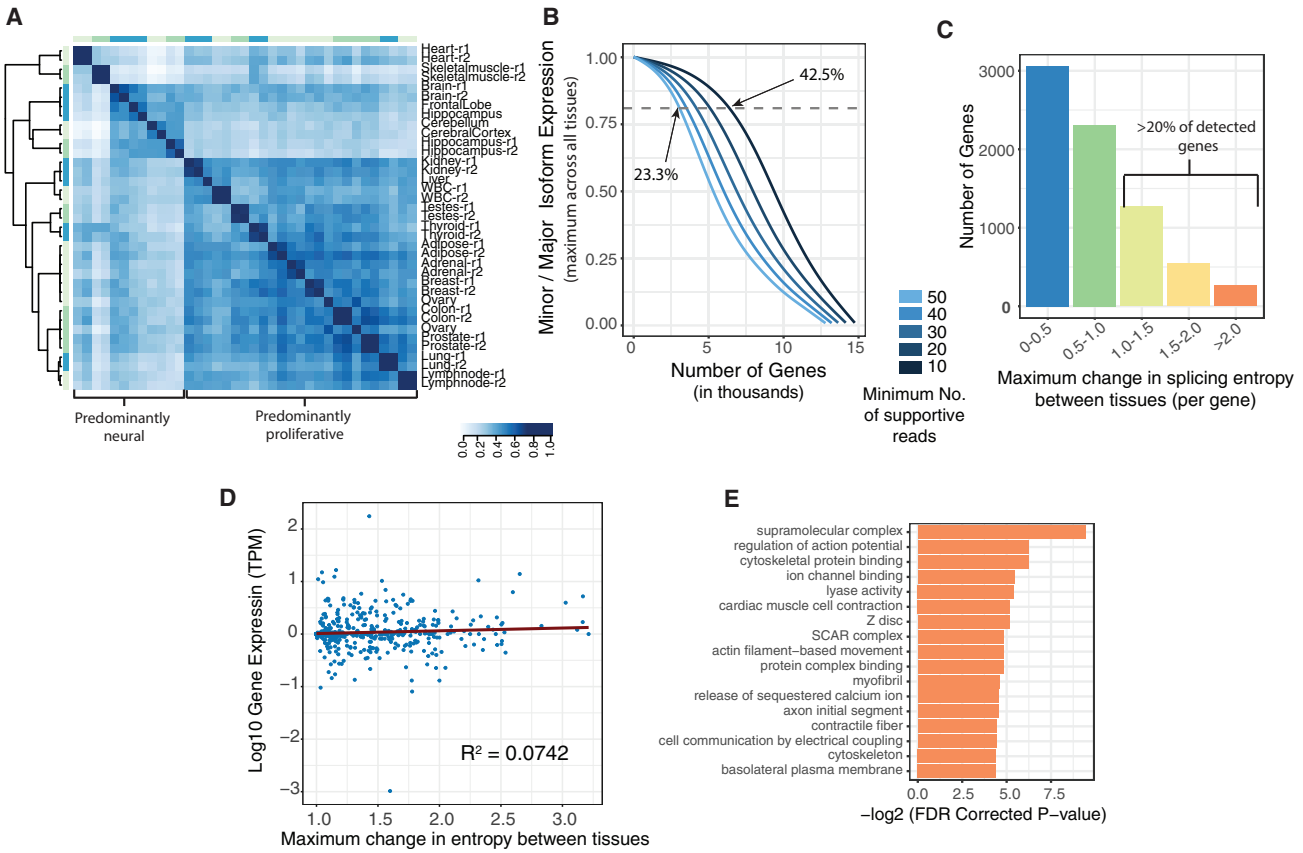

Figure 3. Tissue Regulation of High-Entropy Events Detected using Whippet

(A) Symmetrical heatmap of pairwise correlations of normalized splicing entropy scores across multiple human tissues. Heatmap shows affinity propagation clustering of pairwise similarities between entropy scores. Colored bars surrounding heatmap indicate clusters defined by the dendrogram. Darker blue, stronger correlation in splicing entropy; lighter blue, weak or no correlation. r1, replicate 1; r2, replicate 2.

(B) Plot of ranked genes (x axis) ordered by their maximum minor:major isoform relative expression ratio across all tissues (y axis) at different minimum cut-offs (color scale), for the number of reads mapping to exon-exon junctions corresponding to the AS event. Dashed line, 45:55% ratio cutoff (equivalent to a minor:major ratio of 0.818; see STAR Methods).

(C) Bar plot displaying maximum change in splicing entropy per gene (n = 11,421), revealing that >20% of genes exhibit extensive variance in AS entropy across human tissues. Genes lacking major changes in entropy are not shown.

(D) Scatterplots of change in AS entropy across tissues versus change in expression level of the corresponding genes. Red line, best-fit linear regression. R-squared value calculated using Pearson correlation coefficient.

(E) Functional analysis for GO, REACTOME, and KEGG functional categories of genes with large changes in splicing entropy (>2.0) across human tissues. P value, corrected FDR hypergeometric test.

(Figure 3D; R^2 = 0.074, Pearson correlation). These results contrast with previous proposals that the vast majority of mammalian genes express a single major splice variant (González-Porta et al., 2013; Tress et al., 2017), and instead are consistent with data indicating that a substantial fraction of genes express multiple major isoforms either within or between different cell and tissue types (Tapial et al., 2017; Vaquero-Garcia et al., 2016; Wang et al., 2008). However, new isoforms generated by high entropy AS events detected by Whippet further increase the estimated fraction of genes predicted to express multiple major isoforms compared to previous estimates (e.g., up to ~40% versus ~18% in Tapial et al., 2017). Supporting the possible biological relevance of these AS events, the corresponding genes are enriched in functions associated with the cytoskeleton, extracellular matrix organization, cell communication, signaling, and muscle biology (Figure 3E, p values < 0.05; FDR corrected).

To further investigate the possible significance of high-entropy AS events detected by Whippet, we analyzed their evolutionary conservation using RNA-seq data from six of the same tissues from seven vertebrate species (Brawand et al., 2011), comparing entropy values for the orthologous exons (1,304 "low-entropy" [<1.0] and 369 "high-entropy" [>1.5] exons; Figures 4A, S6D, and S6E) in each species. This revealed a significantly greater concordance in both Ψ and entropy values for orthologous AS events between the analyzed species than expected by chance when compared to randomly permuted sets of exons from the same data (Figures 4B and 4C, low-entropy AS events: $p < 2.2 \times 10^{-16}$; high-entropy AS events: $p < 4.3 \times 10^{-4}$, Kolmogorov-Smirnov test; Figures S6F and S6G; see STAR Methods).

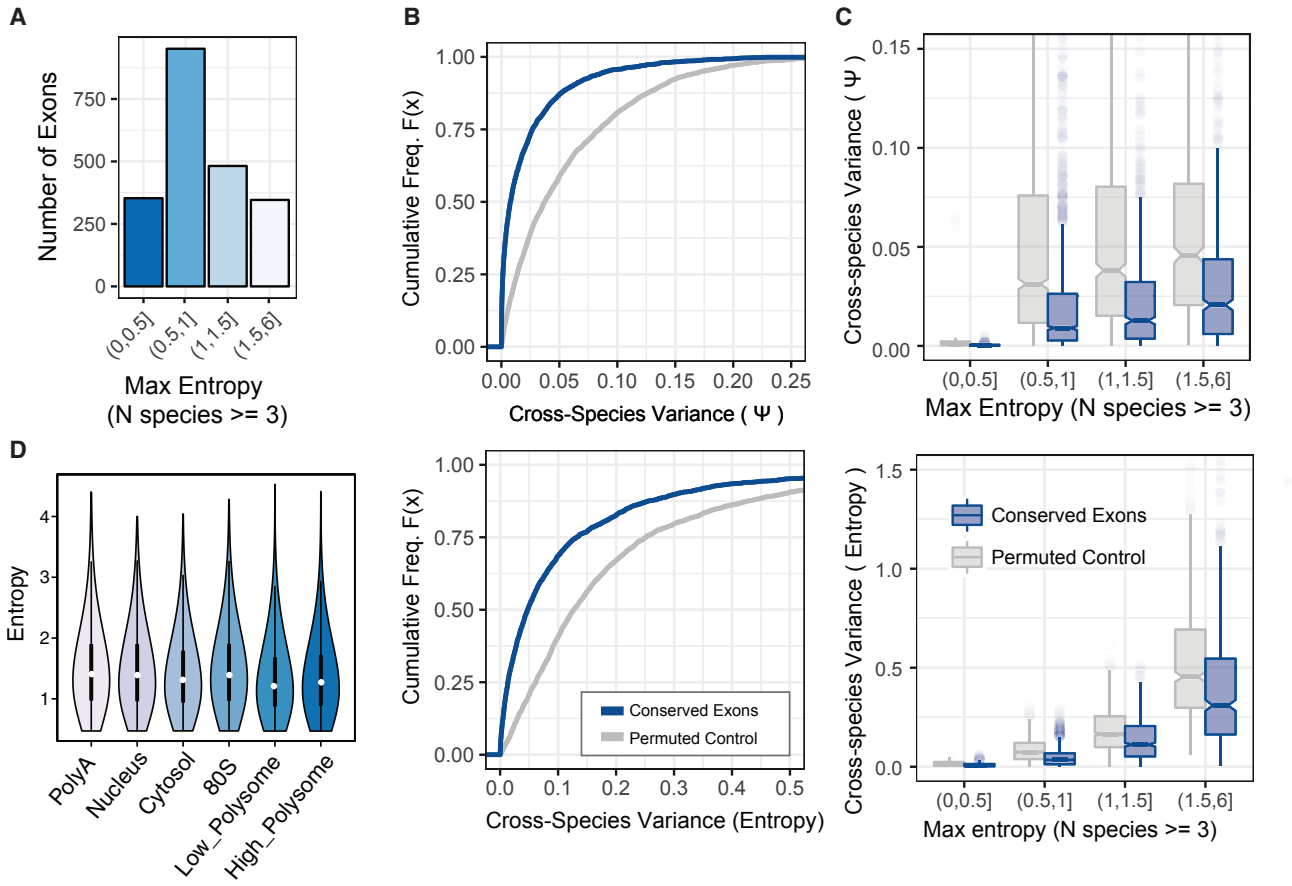

Figure 4. Alternative Splicing Entropy Is Evolutionarily Conserved, and High-Entropy Events Are Potentially Translated

(A) Distribution of the number of unique conserved exons with genomic coordinate "liftover" across at least three vertebrate species (human, chimp, gorilla, mouse, opossum, platypus, and chicken). Conserved exons are counted in discrete bins by their maximum entropy in any of the species.

(B) Cumulative distribution plots comparing the cross-species variance of entropy values among the same tissue in seven vertebrates (at least three species present per event) as compared to a permuted null control. See Figure 2A legend for a description of cumulative distribution plots.

(C) Distributions for the cross-species variance of entropy values (y axis) for conserved exons, binned by maximal entropy values (x axis) and compared to a control set of the same data but with permuted AS event labels for each species (color scale). All two-sided KS-test p values are less than epsilon (2.2×10^{-16}), except for the bin [1.5,3] whose p value was 4.6×10^{-4}. Bottom: same as top, except the distributions plotted contain the cross-species variance of Ψ values (y axis) for the same conserved exons. All two-sided KS-test p values are less than epsilon (2.2×10^{-16}), except for the bin [1.5,3] whose p value was 4.3×10^{-2}. Boxplots display the interquartile range as a solid box, 1.5 times the interquartile range as vertical thin lines, the median as a horizontal line, and the confidence interval around the median as a notch.

(D) Violin plots of the distribution of splicing entropy in different cellular compartments and ribosome (monosome and polysome) fractions. Kernel density is displayed as a symmetric curve, with white dots indicating the median, black box the interquartile range, and black lines the 95% confidence interval.

Thus, overall, the degree of entropy of low- and high-complexity AS events detected and quantified by Whippet is conserved across vertebrate species, implying that these patterns may often be functionally important.

We next asked whether these events are potentially translated. Due to the extremely limited coverage of currently available mass spectrometry data (Blencowe, 2017), Whippet was applied to RNA-seq data from HeLa mono- and polysomes as well as from whole-cell, nuclear, and cytosolic fractions (Floor and Doudna, 2016). This analysis reveals comparable distributions of AS event entropy across all samples (Figure 4D; d < 0.25, Cohen's D statistic, nuclear versus high polyribosome), suggesting that high-entropy AS events contribute substantially to the translated transcriptome. Furthermore, the enrichment of high-entropy AS events within the 5′ UTRs of transcripts (Figure S6H, $p < 4.37 \times 10^{-38}$, Fisher's exact test) suggests possible roles in the regulation of translation.

High-Entropy Alternative Splicing Regulates Genes with Extensive Domain Repeats and Disordered Regions

Given previous evidence for important roles of AS in rewiring protein-protein interaction networks, among other functions (Buljan et al., 2012; Ellis et al., 2012; Yang et al., 2016), we next investigated whether increasing levels of AS-event entropy are associated with specific protein structural features. We observe a significant monotonic increase in the frequency of overlap with

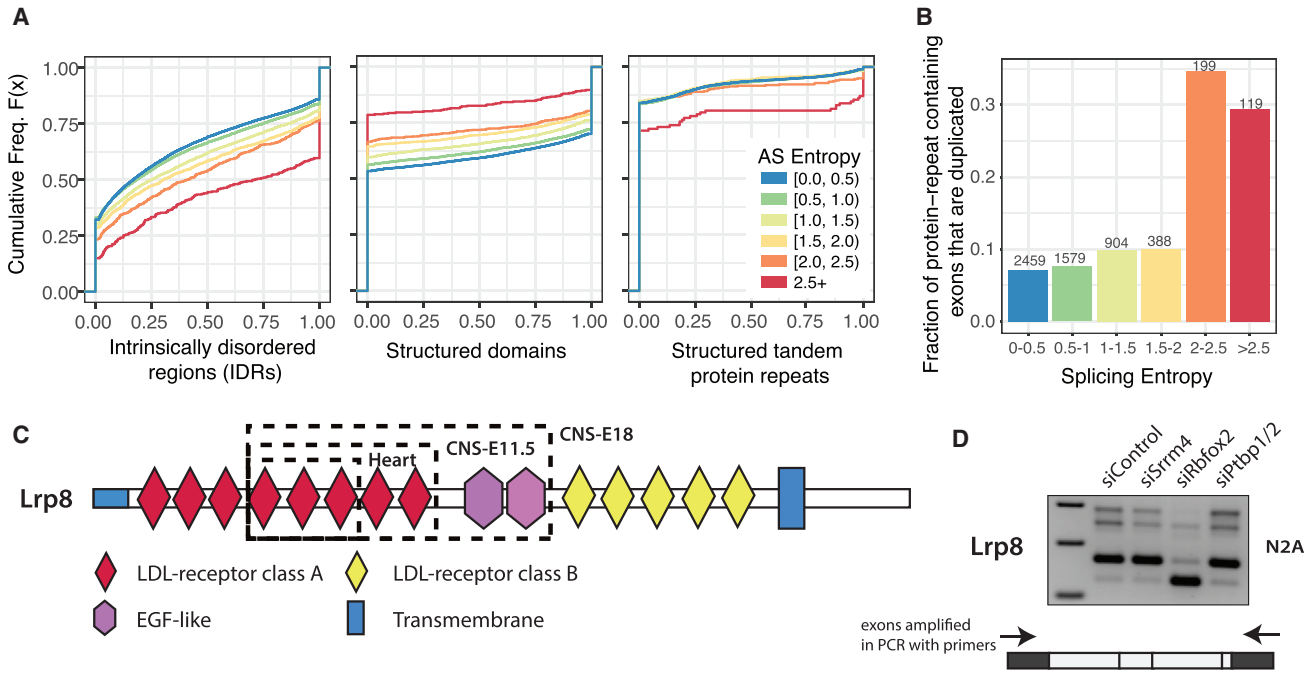

Figure 5. High-Entropy Splicing Events Encode Unique Protein Features

(A) Cumulative distribution plots showing frequency of overlap of AS events (with different degrees of entropy) within intrinsically disordered regions (IDRs) of proteins (left), structured single protein domains (center), and structured tandemly repeated protein domains (right). See Figure 2A legend for a description of the cumulative distribution plots (n > 368).

(B) Bar plot showing frequency at which exons undergoing AS with different degrees of entropy (based on Whippet analysis of tissue RNA-seq data in Figure 3) show evidence of duplication. Numbers of AS events analyzed indicated above plots. See Figure 5A for color legend.

(C) Domain diagram for Lrp8 (low-density lipoprotein receptor-related protein 8) based on SMART annotation. Dotted boxes describe area of proteins undergoing high-entropy splicing in different tissue types. Domain diagram below illustrates exons undergoing splicing within N2a cells and position of primers for RT-PCR validation below. CNS, central nervous system; E, embryonic day; LDL, low-density lipoprotein; EGF, epidermal growth factor.

(D) RT-PCR analysis confirms the presence of putative Lrp8 spliced isoforms in N2a cells. Diagrams below show exon structures of analyzed AS events with approximate positions of RT-PCR primers indicated. See Figure S5 for full gel.

intrinsically disordered regions as a function of increasing entropy of AS events (Figure 5A; $p < 1.02 \times 10^{-43}$, Mann-Whitney U test, low-entropy [<1.0] versus highest-entropy [>2.0] events; Figure S7A). As expected, an inverse trend is observed for overlap with structured domains (Figure 5A, $p < 1.78 \times 10^{-41}$, Mann-Whitney U test). However, an interesting exception is that highest-entropy AS events (entropy > 2.0) display significant overlap with tandem repeat domains (Figure 5A, $p < 2.14 \times 10^{-05}$, Mann-Whitney U test; Figure S7A), particularly nebulin-like and epidermal growth factor (EGF)-like domains (p values < 0.05, Fisher-exact test). Further analysis of the highest-entropy (>2.0) AS events overlapping tandem protein domain repeats reveals that they are significantly more likely to arise from exon duplication than are lower-entropy (<2.0) events (Figure 5B, $p < 4.57 \times 10^{-42}$, Fisher's exact test; Figures S7B and S7C). As an example, high-entropy AS events overlap two classes of tandem repeat domains—LDL-receptor class A and EGF-like domains—within the low-density lipoprotein receptor-related protein 8 (Lrp8). These events were confirmed by RT-PCR analysis (Figure 5C). Moreover, supporting their likely functional importance, one of them is differentially regulated by the neural- and muscle-enriched splicing factor Rbfox2 (Figure 5D). These data thus provide evidence for important roles for Whippet-detected, high-entropy AS events in the expansion of proteomic diversity, principally through changes to intrinsically disordered protein regions and combinatorial changes to the composition of tandem arrays of specific classes of protein domains.

High-Entropy AS Events Display Prototypical Alternative Splicing Signals

We hypothesized that high-entropy AS events may be associated with specific sequence features that facilitate their complex patterns of regulation. To investigate this, we binned AS events by entropy and compared the strengths of their 3′- and 5′-splice sites, flanking intron lengths, and exonic splicing enhancer (ESE) and silencer (ESS) motif densities. Interestingly, the highest-entropy AS events show significant decreases in 3′- and 5′-splice site strength compared to low-entropy AS events (Figure 6A; $p < 3.73 \times 10^{-4}$ and 1.83×10^{-3}, Mann-Whitney U test). Additionally, we observe monotonic decreases in flanking intron length (Figure 6B, $p < 1.78 \times 10^{-18}$, Mann-Whitney U test, highest versus lowest entropy events) and ESS motif density (Figure 6C; ESS: $p < 6.06 \times 10^{-05}$; Mann-Whitney U test, highest versus lowest entropy events) as a function of increasing

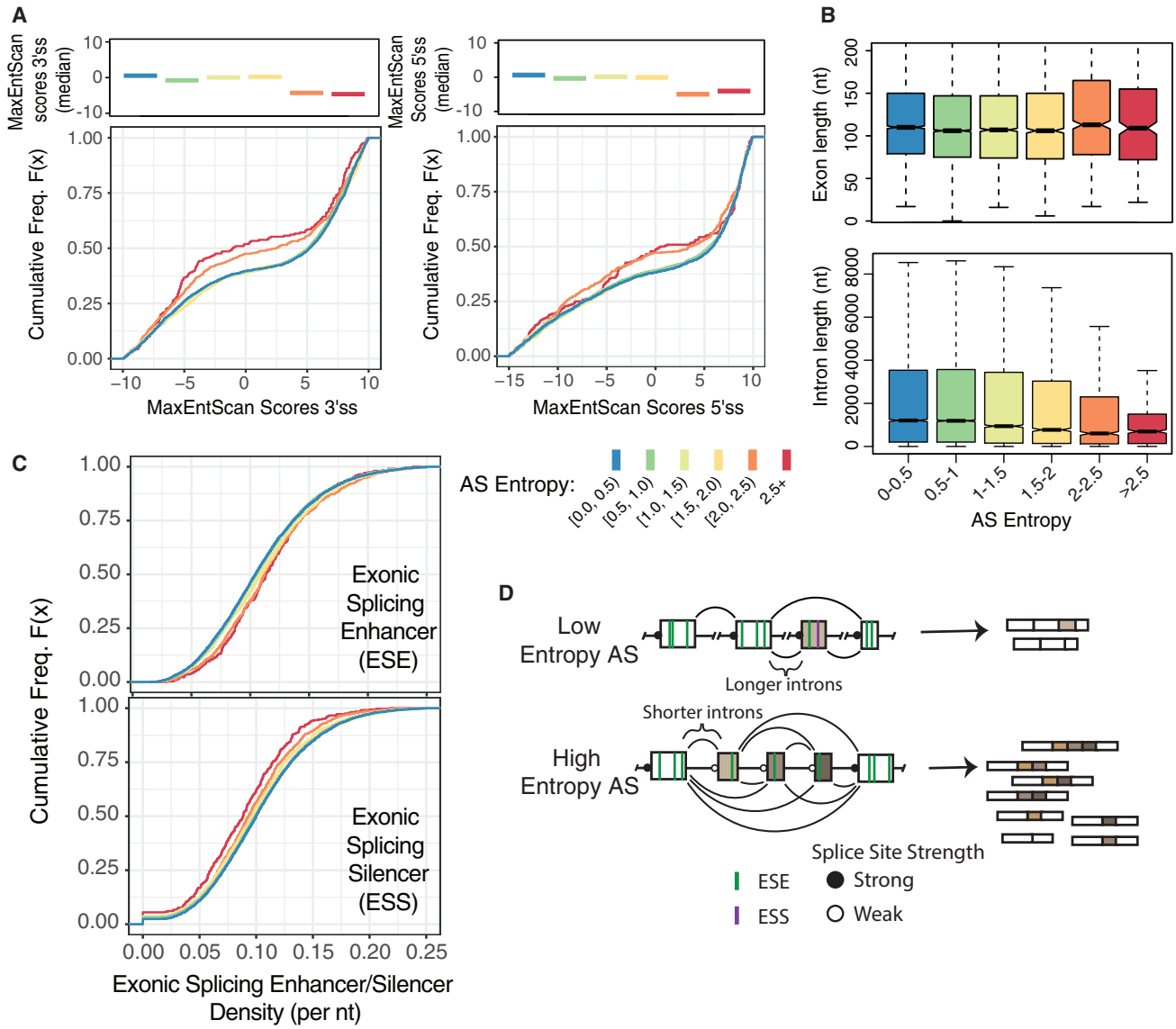

Figure 6. Exons within High-Entropy Splicing Events Have Unique Splice Site Features

(A) Plots showing the cumulative distribution of 3′-splice site (3′ss) strength (left) and 5′-splice site (5′ss) strength (right) estimated using MaxEntScan (Yeo and Burge, 2004) and binned by maximum splicing entropy scores (bottom). The median 3′ss strength for AS events with different degrees of splicing entropy are plotted as colored lines (top). See Figure 2A legend for a description of cumulative distribution plots (n > 1,064).

(B) Boxplot displaying the distribution of exon length (top) and intron length (bottom) surrounding exons binned by maximum entropy of AS. See Figure 6A for color legend. nt, nucleotide; n as in Figure 6A. See Figure 4C for descriptions of boxplots.

(C) Cumulative distribution plots of exonic splicing regulatory elements in AS events with different degrees of AS event entropy. Scores calculated based on the density of exonic splicing enhancers (top) and exonic splicing silencers (bottom) per nucleotide (see STAR Methods). Motifs extracted from Ke et al. (2011). See Figure 6A for color legend and Figure 2A legend for a description of cumulative distribution plots. n as in Figure 6A.

(D) Mechanistic model for the regulation of low-entropy (simple binary) AS events versus high-entropy (complex) AS events by *cis*-regulatory elements and other sequence features. Exons are represented by boxes and introns by lines, with *cis*-regulatory elements and relative splice-site strength indicated by color.

entropy. In contrast, the density of ESE elements displayed a monotonic increase between low- and high-entropy AS events (Figure 6C; ESE: $p < 4.20 \times 10^{-06}$, Mann-Whitney U test, lowest versus highest entropy events). These results suggest that weak splice sites, reduced intronic length, and altered frequencies of exonic splicing elements, are important features underlying the regulation and function of high-entropy AS events (Figure 6D).

Global Increases in High-Entropy AS in Cancer

Aberrant splicing is a hallmark of cancer and contributes to numerous aspects of tumor biology (Ladomery, 2013; Oltean and Bates, 2014). Cancer-associated changes in AS have been linked to altered expression of RNA binding proteins, some of which are oncogenic or act as tumor suppressors, as well as to splicing-sensitive disease mutations that impact the

levels or activities of other cancer-associated genes (Sebestyén et al., 2016; Sterne-Weiler and Sanford, 2014). Despite extensive evidence for altered AS in cancer (Climente-González et al., 2017; Dvinge et al., 2016), the extent to which these changes relate to altered levels of splicing complexity has not been previously determined. Accordingly, we applied Whippet to compare AS entropy using RNA-seq data (Table S3) from 15 matched tumor and control liver samples of patients with hepatocellular carcinoma (HCC), the third leading cause of cancer deaths worldwide. Remarkably, this analysis revealed a significant and reproducible (i.e., between replicate samples) increase in AS event entropy and number of unannotated alternative exon-exon junctions detected in tumor compared to control samples (Figures 7A–7C; Figure S7D; $p < 4.30 \times 10^{-18}$, Mann-Whitney U test), with only a relatively small degree of correlating change in the expression levels of the corresponding genes (Figure S7E; $R^2 = 0.412$, Pearson correlation coefficient). Genes with the largest AS entropy changes display significant enrichment for functions known to be dysregulated in liver cancer, including DNA repair and cell-cycle regulation (Figure 7D; p values < 0.05; FDR corrected).

Further investigation revealed AS events previously identified as aberrant in cancer samples (Figure 7E), including those associated with overexpression of the splicing regulator SRSF1 (Anczuków et al., 2015; Das and Krainer, 2014). Consistent with this observation, differential gene expression analysis revealed a number of RNA-binding proteins, including SRSF1, that are significantly overexpressed in tumor compared to control samples (Figures 7F, 7G, and S7F; DESeq2, FDR corrected p values < 0.01). To further investigate the possible role of SRSF1 overexpression in the expansion of AS entropy observed in the cancer samples, we used Whippet to analyze RNA-seq data (Anczuków et al., 2015) from an MCR-10A cell line overexpressing SRSF1. This revealed a significant increase in high-entropy AS events associated with SRSF1 overexpression (Figure 7H; $p < 9.41 \times 10^{-9}$, Mann-Whitney U test, compared to control) and a significant overlap with events differentially regulated between tumor versus normal tissues (Figure 7I; $p < 2.09 \times 10^{-5}$, Fisher's exact test). These data thus indicate that overall splicing entropy increases in specific tumor types in response to changes in the expression of oncogenic splicing regulators, such as SRSF1. These results further illustrate how Whippet's unique capacity for the efficient and quantitatively accurate profiling of high entropy AS patterns can provide insight into how transcriptomes are altered in different biological contexts.

DISCUSSION

Advancements in RNA-seq analysis have involved the generation of tools that estimate Ψ values from transcript-level expression information (Trincado et al., 2018). While such methods are efficient, we observe that they are subject to increased error rates as a result of inaccuracies in standard transcript annotation models. In contrast, event-level tools are insensitive to distal annotation inaccuracies, since they only consider reads that directly map to splice junctions, exons, or introns forming an AS event. In the present study, we describe Whippet, a graph- and indexing-based, event-level approach for the rapid and accurate quantitative profiling of AS. Whippet applies the concept of lightweight algorithms (Bray et al., 2016; Patro et al., 2014) to splicing quantification using RNA-seq data. As such, it eliminates the requirement for extensive computational resources typically required for read alignment steps. It further affords an unprecedented degree of accuracy in the profiling of complex AS events, in part through the use of entropy as metric for the formalized analysis of AS complexity. Collectively, these attributes of Whippet facilitated the discovery and characterization of transcriptomic complexity and associated features in the present study.

Our results indicate that high-entropy AS events occur more frequently in vertebrate transcriptomes than previously appreciated (Nellore et al., 2016; Vaquero-Garcia et al., 2016), affecting up to 40% of human genes. In contrast to previous proposals that the vast majority of mammalian genes express a single major splice isoform (Gonzàlez-Porta et al., 2013; Tress et al., 2017), our results from employing Whippet reveal that at least one-third of human and mouse genes simultaneously express multiple major isoforms. The results further suggest that many of these events are biologically significant, since their AS entropy levels are frequently tissue-regulated and conserved and the corresponding variant transcripts are highly expressed.

Previously documented examples of high-entropy AS events include those that control the biophysical properties of giant proteins that form muscle fibers (Buck et al., 2010; Li et al., 2012). Many of the high-entropy events detected by Whippet are also reminiscent of well-studied examples in other systems, such as the splice variants generated by tandem arrays of alternative exons in the *Drosophila DSCAM* gene (Bolisetty et al., 2015). In this example, high-entropy AS events overlap tandemly repeated immunoglobulin-like domains that function as interaction surfaces in neural circuit assembly (Hattori et al., 2008). Our results suggest that the targeting of tandemly repeated domains by high-entropy AS may represent a widely used mechanism to modulate the functions of multi-domain proteins. We further provide evidence that large repertoires of transcripts from high-entropy AS events are particularly prominent in post-mitotic tissues, and likely contribute to intricate networks of regulation and cell-cell interactions in these tissues.

Alterations in splicing by spliceosomal gene mutations and overexpression of RBPs contribute to the transcriptomic dysfunction characteristics of myelodysplastic syndromes and related cancers (Inoue et al., 2016). We demonstrate a significant increase in AS event entropy in hepatocellular carcinoma, affecting genes that function in DNA damage and spindle formation, and relate these changes to the mis-regulation of the splicing factor SRSF1. These data may reflect an overall loss of splicing fidelity in cancers and exemplify how the formalization of AS entropy is important when evaluating changes in global splicing patterns (Ritchie et al., 2008). For example, such measures of entropic splicing change may be valuable in future diagnostic techniques for precision medicine.

In summary, Whippet enables the efficient and accurate profiling of simple to complex AS events. As such, it is expected to significantly facilitate future biomedical research. Whippet's ability to rapidly quantify raw read data as a stand-alone

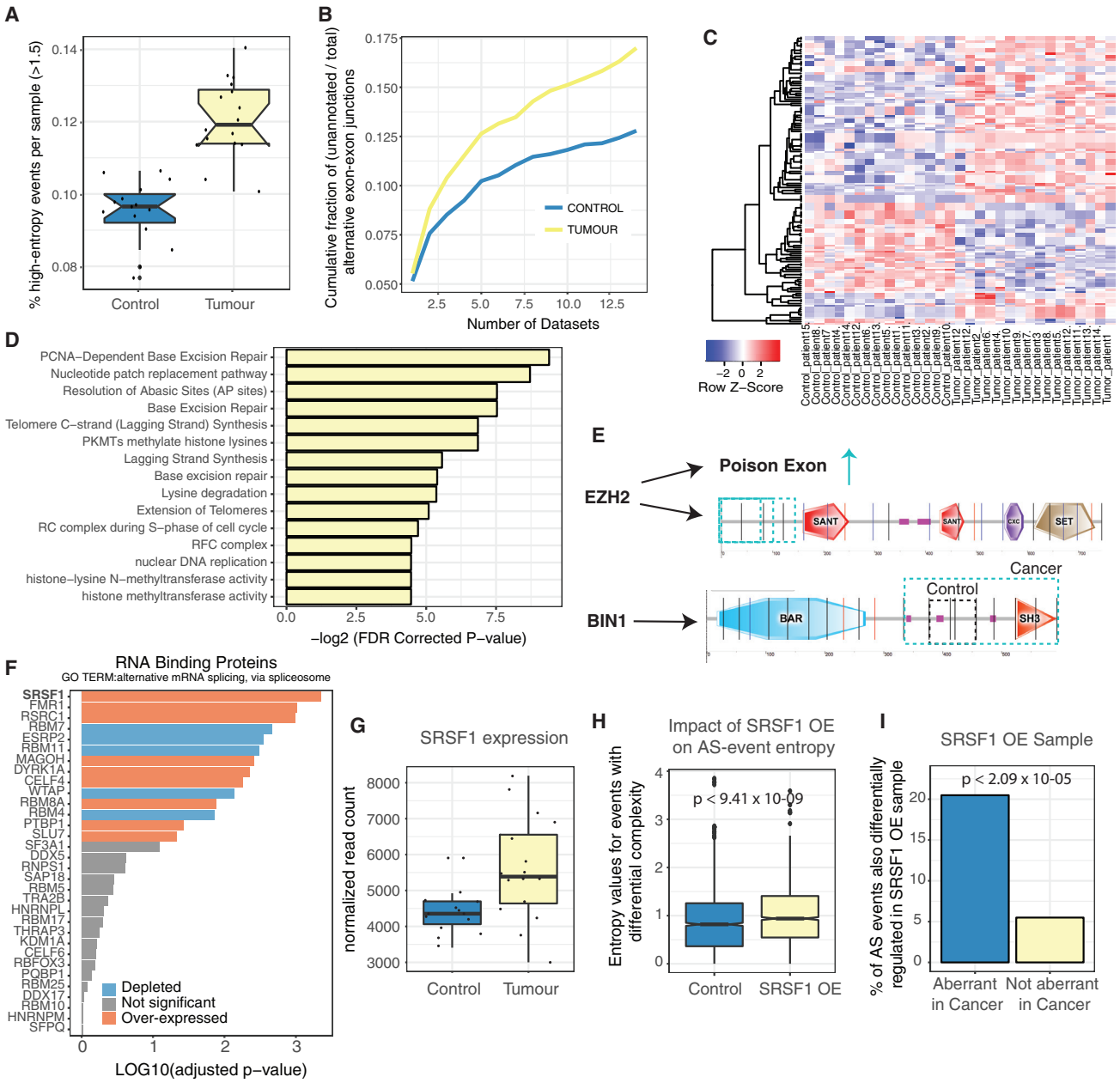

Figure 7. Increases in High-Entropy Splicing in Cancer Are Associated with Overexpression of the Essential Splicing Factor SRSF1

(A) Boxplot showing percentage of high-entropy AS events (> 1.5) within each replicate identified from Whippet analysis of RNA-seq data comprising 15 matched tumor and control samples. Black dots represent individual datasets. See Figure 4C for descriptions of boxplots.

(B) Cumulative proportion of unannotated alternative splice junctions (with two or more supporting reads) identified across matched tumor and control RNA-seq samples. See Figure 2A legend for description of cumulative distribution plots.

(C) Heatmap of splicing entropy values for events with significant changes ($p < 0.05$, Mann-Whitney U test) between tumor and control samples (n = 657).

(D) Bar plots of enriched functional categories for genes harboring AS events with significant entropy changes (p values < 0.05, Mann-Whitney U test) from (C) identified from RNA-seq analysis of 15 matched tumor and control samples. P values were corrected using false discovery rate (FDR) multiple hypothesis testing correction (n = 657).

(E) Schematic diagrams of two genes showing significant changes in AS event entropy between tumor and matched control samples. Domain structure extracted from SMART database. Light blue arrows and boxes indicate increased occurrence of splicing regulation in tumor samples. For BIN1, dashed boxes indicate protein regions predicted to be regulated by splicing in control (gray box) and cancer samples (cyan box). EZH2, Histone-lysine N-methyltransferase EZH2; BIN1, Myc box-dependent-interacting protein 1.

(F) Differential gene expression analysis for selected RNA-binding proteins (GO:0000380) identified from RNA-seq analysis of 15 matched tumor and control samples. Genes with blue bars display reduced expression in cancer samples, red bars show increased expression in cancer samples, and gray bars show no significant difference between control and tumor samples.

(legend continued on next page)

software package on a personal computer further renders genome-wide analyses of AS more accessible to the scientific community. In this regard, we believe that Whippet will represent a valuable tool until long-read sequencing protocols (Byrne et al., 2017; Tilgner et al., 2018) offer comparable sequencing depth and efficiency as short-read analysis methods.

Limitations

A limitation of Whippet is that it only detects and analyzes AS events represented by splice sites in a CSG index. However, it can detect and quantify previously unknown AS events representing novel combinations of splice junctions derived from the indexed splice sites. Moreover, CSG indices can be supplemented beyond standard annotation sets with new splice sites (and therefore novel exons) mined using *de novo* spliced read aligners (Dobin et al., 2013; Kim et al., 2015; see Methods S1 and Figure S1E). This approach is expected to be useful in the analysis of AS from poorly annotated species as well as disease-altered transcriptomes harboring aberrant splicing patterns.

STAR★METHODS

Detailed methods are provided in the online version of this paper and include the following:

- KEY RESOURCES TABLE
- CONTACT FOR REAGENT AND RESOURCE SHARING
- EXPERIMENTAL MODEL AND SUBJECT DETAILS
  - Cell lines and Cell Culture
  - Short interfering RNA knockdown and RT-PCR
- METHOD DETAILS
  - RNA-seq simulation
  - Combinatorial gene model
  - Benchmarking
  - Tissue-wide analysis of splicing
  - Feature analysis of high-entropy AS events
  - Analysis of cancer data
- QUANTIFICATION AND STATISTICAL ANALYSIS
  - Contiguous splice graph index
  - AS event definition and PSI quantification
  - Whippet_TPM
  - Statistical analysis
  - Additional resources
- DATA AND SOFTWARE AVAILABILITY

SUPPLEMENTAL INFORMATION

Supplemental Information includes Methods S1, seven figures, and seven tables and can be found with this article online at https://doi.org/10.1016/j.molcel.2018.08.018.

ACKNOWLEDGMENTS

We gratefully acknowledge M. Irimia and P. Melsted for valuable suggestions and testing of the Whippet software. We also thank G. Bader, N. Barbosa-Morais, U. Braunschweig, S. Gueroussov, T. Gonatopoulos-Pourtnatzis, and B. Harpur for helpful discussions and comments of the manuscript. This work was supported by grants from The Canadian Institutes of Health Research CIHR and Canada First Excellence Fund to B.J.B. Additional support was provided by CIHR postdoctoral fellowships (T.S.W., R.J.W., and A.B.), a C.H. Best Postdoctoral Fellowship (T.S.-W.), a Marie Curie IOF Fellowship (R.J.W.), an EMBO Long-Term Fellowship (A.J.B.), an Ontario Graduate Scholarship, and a CIHR Frederick Banting and C.H. Best Canada Graduate Scholarship (K.C.H.H.). B.J.B. holds the University of Toronto Banbury Chair in Medical Research.

AUTHOR CONTRIBUTIONS

T.S.-W., with contributions from R.J.W., conceived, designed, and implemented the Whippet software. T.S.-W., R.J.W., and K.C.H.H. simulated data and benchmarked accuracy and performance. R.J.W. and T.S.-W., with input from B.J.B., designed and performed computational analyses. A.J.B. performed experimental validations. T.S.-W, R.J.W, and B.J.B. wrote the manuscript with input from the other authors.

DECLARATION OF INTERESTS

The authors declare no competing interests.

Received: April 13, 2018
Revised: June 24, 2018
Accepted: August 9, 2018
Published: September 13, 2018

SUPPORTING CITATIONS

The following references appear in the Supplemental Information: Hansen et al. (2010); Letunic et al. (2002); Love et al. (2016); Pachter (2011); Roberts et al. (2011).

REFERENCES

Anczuków, O., Akerman, M., Cléry, A., Wu, J., Shen, C., Shirole, N.H., Raimer, A., Sun, S., Jensen, M.A., Hua, Y., et al. (2015). SRSF1-Regulated Alternative Splicing in Breast Cancer. Mol. Cell *60*, 105–117.

Baralle, F.E., and Giudice, J. (2017). Alternative splicing as a regulator of development and tissue identity. Nat. Rev. Mol. Cell Biol. *18*, 437–451.

Blencowe, B.J. (2017). The Relationship between Alternative Splicing and Proteomic Complexity. Trends Biochem. Sci. *42*, 407–408.

Bodenhofer, U., Kothmeier, A., and Hochreiter, S. (2011). APCluster: an R package for affinity propagation clustering. Bioinformatics *27*, 2463–2464.

Bolisetty, M.T., Rajadinakaran, G., and Graveley, B.R. (2015). Determining exon connectivity in complex mRNAs by nanopore sequencing. Genome Biol. *16*, 204.

Brawand, D., Soumillon, M., Necsulea, A., Julien, P., Csárdi, G., Harrigan, P., Weier, M., Liechti, A., Aximu-Petri, A., Kircher, M., et al. (2011). The evolution of gene expression levels in mammalian organs. Nature *478*, 343–348.

Bray, N.L., Pimentel, H., Melsted, P., and Pachter, L. (2016). Near-optimal probabilistic RNA-seq quantification. Nat. Biotechnol. *34*, 525–527.

(G) Boxplot showing normalized read counts for SRSF1. See Figure 4C for descriptions of boxplots.
(H) Boxplot showing relative complexity of transcriptomes as measured by distribution of entropy scores for high-quality AS events, between SRSF1 overexpression (OE) sample and matched control (n = 1,998). Statistical test, Mann-Whitney U test. See Figure 4C for descriptions of boxplots.
(I) Bar plot showing percentage of events from plot (H) with differential splicing changes between SRSF1 OE (overexpression) and matched control samples that overlap with splicing changes in tumor samples from (C), as compared to the number of overlapping events expected by chance (n = 1,998). Statistical test, Fisher's exact test.

Buck, D., Hudson, B.D., Ottenheijm, C.A., Labeit, S., and Granzier, H. (2010). Differential splicing of the large sarcomeric protein nebulin during skeletal muscle development. J. Struct. Biol. *170*, 325–333.

Buljan, M., Chalancon, G., Eustermann, S., Wagner, G.P., Fuxreiter, M., Bateman, A., and Babu, M.M. (2012). Tissue-specific splicing of disordered segments that embed binding motifs rewires protein interaction networks. Mol. Cell *46*, 871–883.

Byrne, A., Beaudin, A.E., Olsen, H.E., Jain, M., Cole, C., Palmer, T., DuBois, R.M., Forsberg, E.C., Akeson, M., and Vollmers, C. (2017). Nanopore long-read RNAseq reveals widespread transcriptional variation among the surface receptors of individual B cells. Nat. Commun. *8*, 16027.

Climente-González, H., Porta-Pardo, E., Godzik, A., and Eyras, E. (2017). The Functional Impact of Alternative Splicing in Cancer. Cell Rep. *20*, 2215–2226.

Das, S., and Krainer, A.R. (2014). Emerging functions of SRSF1, splicing factor and oncoprotein, in RNA metabolism and cancer. Mol. Cancer Res. *12*, 1195–1204.

Dobin, A., Davis, C.A., Schlesinger, F., Drenkow, J., Zaleski, C., Jha, S., Batut, P., Chaisson, M., and Gingeras, T.R. (2013). STAR: ultrafast universal RNA-seq aligner. Bioinformatics *29*, 15–21.

Dosztányi, Z., Csizmok, V., Tompa, P., and Simon, I. (2005). IUPred: web server for the prediction of intrinsically unstructured regions of proteins based on estimated energy content. Bioinformatics *21*, 3433–3434.

Dvinge, H., Kim, E., Abdel-Wahab, O., and Bradley, R.K. (2016). RNA splicing factors as oncoproteins and tumour suppressors. Nat. Rev. Cancer *16*, 413–430.

Ellis, J.D., Barrios-Rodiles, M., Colak, R., Irimia, M., Kim, T., Calarco, J.A., Wang, X., Pan, Q., O'Hanlon, D., Kim, P.M., et al. (2012). Tissue-specific alternative splicing remodels protein-protein interaction networks. Mol. Cell *46*, 884–892.

Ferragina, P., Manzini, G., Mäkinen, V., and Navarro, G. (2004). An alphabet-friendly FM-index. In String Processing and Information Retrieval: 11th International Conference, SPIRE 2004, Padova, Italy, October 5-8, 2004 Proceedings, A. Apostolico, and M. Melucci, eds. (Berlin, Heidelberg: Springer Berlin Heidelberg), pp. 150–160.

Floor, S.N., and Doudna, J.A. (2016). Tunable protein synthesis by transcript isoforms in human cells. eLife *5*, e10921.

Frazee, A.C., Jaffe, A.E., Langmead, B., and Leek, J.T. (2015). Polyester: simulating RNA-seq datasets with differential transcript expression. Bioinformatics *31*, 2778–2784.

Gonzàlez-Porta, M., Frankish, A., Rung, J., Harrow, J., and Brazma, A. (2013). Transcriptome analysis of human tissues and cell lines reveals one dominant transcript per gene. Genome Biol. *14*, R70.

Grant, G.R., Farkas, M.H., Pizarro, A.D., Lahens, N.F., Schug, J., Brunk, B.P., Stoeckert, C.J., Hogenesch, J.B., and Pierce, E.A. (2011). Comparative analysis of RNA-Seq alignment algorithms and the RNA-Seq unified mapper (RUM). Bioinformatics *27*, 2518–2528.

Hansen, K.D., Brenner, S.E., and Dudoit, S. (2010). Biases in Illumina transcriptome sequencing caused by random hexamer priming. Nucleic Acids Res. *38*, e131.

Hattori, D., Millard, S.S., Wojtowicz, W.M., and Zipursky, S.L. (2008). Dscam-mediated cell recognition regulates neural circuit formation. Annu. Rev. Cell Dev. Biol. *24*, 597–620.

Heber, S., Alekseyev, M., Sze, S.H., Tang, H., and Pevzner, P.A. (2002). Splicing graphs and EST assembly problem. Bioinformatics *18* (*Suppl 1*), S181–S188.

Inoue, D., Bradley, R.K., and Abdel-Wahab, O. (2016). Spliceosomal gene mutations in myelodysplasia: molecular links to clonal abnormalities of hematopoiesis. Genes Dev. *30*, 989–1001.

Irimia, M., Weatheritt, R.J., Ellis, J.D., Parikshak, N.N., Gonatopoulos-Pournatzis, T., Babor, M., Quesnel-Vallières, M., Tapial, J., Raj, B., O'Hanlon, D., et al. (2014). A highly conserved program of neuronal microexons is misregulated in autistic brains. Cell *159*, 1511–1523.

Katz, Y., Wang, E.T., Airoldi, E.M., and Burge, C.B. (2010). Analysis and design of RNA sequencing experiments for identifying isoform regulation. Nat. Methods *7*, 1009–1015.

Ke, S., Shang, S., Kalachikov, S.M., Morozova, I., Yu, L., Russo, J.J., Ju, J., and Chasin, L.A. (2011). Quantitative evaluation of all hexamers as exonic splicing elements. Genome Res. *21*, 1360–1374.

Kim, D., Pertea, G., Trapnell, C., Pimentel, H., Kelley, R., and Salzberg, S.L. (2013). TopHat2: accurate alignment of transcriptomes in the presence of insertions, deletions and gene fusions. Genome Biol. *14*, R36.

Kim, D., Langmead, B., and Salzberg, S.L. (2015). HISAT: a fast spliced aligner with low memory requirements. Nat. Methods *12*, 357–360.

Ladomery, M. (2013). Aberrant alternative splicing is another hallmark of cancer. Int. J. Cell Biol. *2013*, 463786.

Letunic, I., Copley, R.R., and Bork, P. (2002). Common exon duplication in animals and its role in alternative splicing. Hum. Mol. Genet. *11*, 1561–1567.

Letunic, I., Doerks, T., and Bork, P. (2015). SMART: recent updates, new developments and status in 2015. Nucleic Acids Res. *43*, D257–D260.

Li, B., and Dewey, C.N. (2011). RSEM: accurate transcript quantification from RNA-Seq data with or without a reference genome. BMC Bioinformatics *12*, 323.

Li, S., Guo, W., Schmitt, B.M., and Greaser, M.L. (2012). Comprehensive analysis of titin protein isoform and alternative splicing in normal and mutant rats. J. Cell. Biochem. *113*, 1265–1273.

Liu, Y., Gonzàlez-Porta, M., Santos, S., Brazma, A., Marioni, J.C., Aebersold, R., Venkitaraman, A.R., and Wickramasinghe, V.O. (2017). Impact of Alternative Splicing on the Human Proteome. Cell Rep. *20*, 1229–1241.

Love, M.I., Huber, W., and Anders, S. (2014). Moderated estimation of fold change and dispersion for RNA-seq data with DESeq2. Genome Biol. *15*, 550.

Love, M.I., Hogenesch, J.B., and Irizarry, R.A. (2016). Modeling of RNA-seq fragment sequence bias reduces systematic errors in transcript abundance estimation. Nat. Biotechnol. *34*, 1287–1291.

Nellore, A., Jaffe, A.E., Fortin, J.P., Alquicira-Hernández, J., Collado-Torres, L., Wang, S., Phillips, R.A., III, Karbhari, N., Hansen, K.D., Langmead, B., and Leek, J.T. (2016). Human splicing diversity and the extent of unannotated splice junctions across human RNA-seq samples on the Sequence Read Archive. Genome Biol. *17*, 266.

Oltean, S., and Bates, D.O. (2014). Hallmarks of alternative splicing in cancer. Oncogene *33*, 5311–5318.

Pachter, L. (2011). Models for transcript quantification from RNA-seq. arXiv:1104.3889v2.

Pan, Q., Shai, O., Lee, L.J., Frey, B.J., and Blencowe, B.J. (2008). Deep surveying of alternative splicing complexity in the human transcriptome by high-throughput sequencing. Nat. Genet. *40*, 1413–1415.

Patro, R., Mount, S.M., and Kingsford, C. (2014). Sailfish enables alignment-free isoform quantification from RNA-seq reads using lightweight algorithms. Nat. Biotechnol. *32*, 462–464.

Patro, R., Duggal, G., Love, M.I., Irizarry, R.A., and Kingsford, C. (2017). Salmon provides fast and bias-aware quantification of transcript expression. Nat. Methods *14*, 417–419.

Pellegrini, M., Renda, M.E., and Vecchio, A. (2012). Ab initio detection of fuzzy amino acid tandem repeats in protein sequences. BMC Bioinformatics *13* (*Suppl 3*), S8.

Raj, B., Irimia, M., Braunschweig, U., Sterne-Weiler, T., O'Hanlon, D., Lin, Z.Y., Chen, G.I., Easton, L.E., Ule, J., Gingras, A.C., et al. (2014). A global regulatory mechanism for activating an exon network required for neurogenesis. Mol. Cell *56*, 90–103.

Ritchie, W., Granjeaud, S., Puthier, D., and Gautheret, D. (2008). Entropy measures quantify global splicing disorders in cancer. PLoS Comput. Biol. *4*, e1000011.

Roberts, A., Trapnell, C., Donaghey, J., Rinn, J.L., and Pachter, L. (2011). Improving RNA-seq expression estimates by correcting for fragment bias. Genome Biol. *12*, R22.

Sebestyén, E., Singh, B., Miñana, B., Pagès, A., Mateo, F., Pujana, M.A., Valcárcel, J., and Eyras, E. (2016). Large-scale analysis of genome and transcriptome alterations in multiple tumors unveils novel cancer-relevant splicing networks. Genome Res. *26*, 732–744.

Silvester, N., Alako, B., Amid, C., Cerdeño-Tarrága, A., Clarke, L., Cleland, I., Harrison, P.W., Jayathilaka, S., Kay, S., Keane, T., et al. (2018). The European Nucleotide Archive in 2017. Nucleic Acids Res. *46* (D1), D36–D40.

Sterne-Weiler, T., and Sanford, J.R. (2014). Exon identity crisis: disease-causing mutations that disrupt the splicing code. Genome Biol. *15*, 201.

Sterne-Weiler, T., Martinez-Nunez, R.T., Howard, J.M., Cvitovik, I., Katzman, S., Tariq, M.A., Pourmand, N., and Sanford, J.R. (2013). Frac-seq reveals isoform-specific recruitment to polyribosomes. Genome Res. *23*, 1615–1623.

Tapial, J., Ha, K.C.H., Sterne-Weiler, T., Gohr, A., Braunschweig, U., Hermoso-Pulido, A., Quesnel-Vallières, M., Permanyer, J., Sodaei, R., Marquez, Y., et al. (2017). An atlas of alternative splicing profiles and functional associations reveals new regulatory programs and genes that simultaneously express multiple major isoforms. Genome Res. *27*, 1759–1768.

Tilgner, H., Jahanbani, F., Gupta, I., Collier, P., Wei, E., Rasmussen, M., and Snyder, M.P. (2018). Microfluidic isoform sequencing shows widespread splicing coordination in the human transcriptome. Genome Res. *28*, 231–242. Published online December 1, 2017.

Trapnell, C., Williams, B.A., Pertea, G., Mortazavi, A., Kwan, G., van Baren, M.J., Salzberg, S.L., Wold, B.J., and Pachter, L. (2010). Transcript assembly and quantification by RNA-Seq reveals unannotated transcripts and isoform switching during cell differentiation. Nat. Biotechnol. *28*, 511–515.

Tress, M.L., Abascal, F., and Valencia, A. (2017). Most Alternative Isoforms Are Not Functionally Important. Trends Biochem. Sci. *42*, 408–410.

Trincado, J.L., Entizne, J.C., Hysenaj, G., Singh, B., Skalic, M., Elliott, D.J., and Eyras, E. (2018). SUPPA2: fast, accurate, and uncertainty-aware differential splicing analysis across multiple conditions. Genome Biol. *19*, 40.

Vaquero-Garcia, J., Barrera, A., Gazzara, M.R., González-Vallinas, J., Lahens, N.F., Hogenesch, J.B., Lynch, K.W., and Barash, Y. (2016). A new view of transcriptome complexity and regulation through the lens of local splicing variations. eLife *5*, e11752.

Wang, E.T., Sandberg, R., Luo, S., Khrebtukova, I., Zhang, L., Mayr, C., Kingsmore, S.F., Schroth, G.P., and Burge, C.B. (2008). Alternative isoform regulation in human tissue transcriptomes. Nature *456*, 470–476.

Wang, J., Pan, Y., Shen, S., Lin, L., and Xing, Y. (2017). rMATS-DVR: rMATS discovery of differential variants in RNA. Bioinformatics *33*, 2216–2217.

Weatheritt, R.J., Sterne-Weiler, T., and Blencowe, B.J. (2016). The ribosome-engaged landscape of alternative splicing. Nat. Struct. Mol. Biol. *23*, 1117–1123.

Wootton, J.C. (1994). Non-globular domains in protein sequences: automated segmentation using complexity measures. Comput. Chem. *18*, 269–285.

Xiong, H.Y., Lee, L.J., Bretschneider, H., Gao, J., Jojic, N., and Frey, B.J. (2016). Probabilistic estimation of short sequence expression using RNA-Seq data and the positional bootstrap. bioRxiv. https://doi.org/10.1101/046474.

Yang, X., Coulombe-Huntington, J., Kang, S., Sheynkman, G.M., Hao, T., Richardson, A., Sun, S., Yang, F., Shen, Y.A., Murray, R.R., et al. (2016). Widespread Expansion of Protein Interaction Capabilities by Alternative Splicing. Cell *164*, 805–817.

Yeo, G., and Burge, C.B. (2004). Maximum entropy modeling of short sequence motifs with applications to RNA splicing signals. J. Comput. Biol. *11*, 377–394.

STAR★METHODS

KEY RESOURCES TABLE

REAGENT or RESOURCE	SOURCE	IDENTIFIER
Chemicals, Peptides, and Recombinant Proteins		
Lipofectamine RNAiMAX	Invitrogen	Cat# 13778030
SMARTpool siRNAs	Dharmacon	N/A
Critical Commercial Assays		
One-Step RT-PCR	QIAGEN	Cat# 210210
RNeasy Mini Kit	QIAGEN	Cat# 74104
Experimental Models: Cell Lines		
Human: HeLa	N/A	N/A
Mouse: Neuro2A	ATCC	ATCC CCL-131
Deposited Data		
Public RNA-seq data used in paper	Table S3	Table S3
Oligonucleotides		
Slmap: Forward:GAGCGCACTCAGGAAGAGTT Reverse: TTCCTTTGCTTTTGCCTGAT	This paper	N/A
Slmap (Control): Forward:GAGCGCACTCAGGAAGAGTT Reverse:TTCCTGCTCAGTCATTTCAAAC	This paper	N/A
Eps15l1: Forward:TTGGAACCCTAGACCCCTTT Reverse:CTTTTTCACTCTCCCGCTTG	This paper	N/A
Asap1: Forward:GCCCGCGATGGAATAATG Reverse:TGAGGAAGAGGCACAGGTCT	This paper	N/A
Eml4: Forward:TCCTGTATAACCAATGGAAGTG Reverse:CATTGTAATTGGCCGACCTC	This paper	N/A
Atp8a1: Forward:CGGTCGTTACACAACACTGG Reverse:GGCCAAGTTCCTCATTCAGA	This paper	N/A
Sfl1: Forward:TCATGCCTCACAAAACTGGA Reverse:CCATAGCCAGCCTCTGTACC	This paper	N/A
Mapt: Forward:AATGGAAGACCATGCTGGAG Reverse:GCCACACTTGGAGGTCACTT	This paper	N/A
Lrp8: Forward:CGGAGAGAAGGACTGTGAGG Reverse:CAGTGCAGATGTGGGAACAG	This paper	N/A
Gtf2ird1: Forward:CCCCAACACCTATGACATCC Reverse:CGCTTGGGAATGTTGTCTTT	This paper	N/A
Rbms3: Forward:GAGACAGGGTCAGAGCAAGC Reverse:AAACCGGAGGCCAACTAACT	This paper	N/A
Cask: Forward:AGGGAAATGCGAGGGAGTAT Reverse:GTCATCCTTGGCTGGATCAT	This paper	N/A

(*Continued on next page*)

Continued

REAGENT or RESOURCE	SOURCE	IDENTIFIER
Software and Algorithms		
Whippet	This paper	https://github.com/timbitz/Whippet.jl
Whippet_TPM	This paper	https://github.com/timbitz/Whippet.jl
Supplemental scripts and simulated data	This paper	http://figshare.com/articles/Whippet_analysis_scripts/5711683
Julia	N/A	http://www.julialang.org
BioJulia	N/A	https://github.com/BioJulia
MAJIQ	(Vaquero-Garcia et al., 2016)	https://majiq.biociphers.org/
rMATS	(Wang et al., 2017)	http://rnaseq-mats.sourceforge.net/
MISO	(Katz et al., 2010)	http://genes.mit.edu/burgelab/miso/
VAST-TOOLS	(Tapial et al., 2017)	https://github.com/vastgroup/vast-tools
BENTO	(Xiong et al., 2016)	https://github.com/PSI-Lab/BENTO-Seq
SUPPA	(Trincado et al., 2018)	https://github.com/comprna/SUPPA
Kallisto	(Bray et al., 2016)	https://pachterlab.github.io/kallisto/
STAR	(Dobin et al., 2013)	https://github.com/alexdobin/STAR
HISAT	(Kim et al., 2015)	https://ccb.jhu.edu/software/hisat
TOPHAT	(Kim et al., 2013)	http://ccb.jhu.edu/software/tophat
BEERS	(Grant et al., 2011)	http://cbil.upenn.edu/BEERS/
Polyester	(Frazee et al., 2015)	https://github.com/alyssafrazee/polyester
RSEM	(Li and Dewey, 2011)	https://github.com/deweylab/RSEM
DESeq2	(Love et al., 2014)	https://bioconductor.org/packages/release/bioc/html/DESeq2.html
IUPred	(Dosztányi et al., 2005)	http://iupred.enzim.hu/
MaxEntScan	(Yeo and Burge, 2004)	http://genes.mit.edu/burgelab/maxent/Xmaxentscan_scoreseq.html
apcluster	(Bodenhofer et al., 2011)	https://cran.r-project.org/web/packages/apcluster/index.html
PTRStalker	(Pellegrini et al., 2012)	http://bioalgo.iit.cnr.it/index.php?pg=ptrs
SEG	(Wootton, 1994)	http://www.biology.wustl.edu/gcg/seg.html
Image Lab	BioRad	Cat# 1709691
Other		
Parameters for software used	Table S7	Table S7
Supplemental Methods	Methods S1	Methods S1
Additional Benchmarks	Methods S1	Methods S1

CONTACT FOR REAGENT AND RESOURCE SHARING

Requests should be directed to and will be fulfilled by Lead Contact Benjamin Blencowe (b.blencowe@utoronto.ca).

EXPERIMENTAL MODEL AND SUBJECT DETAILS

Cell lines and Cell Culture

Neuro-2A (N2A) cells are a male, mouse neuroblastoma cell line, and were grown in DMEM supplemented with 10% FBS, sodium pyruvate, non-essential amino acids and penicillin/streptomycin. Cells were maintained at 37°C with 5% CO_2. An authenticated N2A cell line was purchased from ATCC (catalog number: ATCC CCL-131).

Short interfering RNA knockdown and RT-PCR

Mouse Neuro2A (N2A) cells were transfected with SMARTpool siRNAs (Dharmacon) (50nM final concentration) using Lipofectamine RNAiMAX (Invitrogen), as recommended by the manufacturer. A non-targeting siRNA pool (siNT) was used as a control. Cells were harvested at 48 hours post transfection and total RNA was extracted using RNeasy columns (QIAGEN). Semi-quantitative RT-PCR

was performed using the QIAGEN One-Step RT-PCR kit as per the manufacturer's instructions, using 50ng total RNA in a 20uL reaction. Products were resolved on 2-4% agarose gels and bands were quantified using Image Lab (BioRad) or ImageJ. Predictions of band sizes were based on *in silico* PCR using data from the UCSC Genome Browser (http://genome.ucsc.edu) server after combining exons from Whippet predictions. Only predictions supported by multiple sources of evidence (i.e. RT-PCR, Whippet and UCSC) were included in figures (see **Key Resources Table** for details of primers used).

METHOD DETAILS

RNA-seq simulation

To simulate RNA-seq reads transcriptome wide, we used RSEM (Li and Dewey, 2011) to quantify the benchmark dataset SRR2300536 (a ~25M read depth RNA-seq dataset from HeLa cell line). With the RSEM parameters and gene expression distributions obtained from this quantification (RSEM *estimated_model_file*, *estimated_isoform_results,* and *theta*), we used RSEM's *rsem-simulate-reads* to simulate 50M paired-end reads for each of two hg19 annotation builds: Gencode v25 TSL1, and RefSeq Release 84. In order to calculate 'ground truth' (i.e., known) Ψ values for Whippet nodes, we used the Whippet_TPM method on the ground truth isoform TPM values provided by the RSEM simulator.

To investigate the accuracy and capability of AS quantification tools, we simulated transcripts with AS-events of increasing complexity. To formalize AS events into discrete classes of complexity K(n) = 2^n splicing-outcomes for K1 through K6, we randomly chose 500 CSGs of each complexity class with at least n total internal nodes (not including nodes with TxStart or TxEnd node boundaries). From those CSGs, we randomly chose a set of n consecutive internal nodes and created partial transcript sequences from the first internal node to the last internal node, with all combinations of n internal nodes. In the case of nodes with Soft boundary types, less than 2^n total combinations were created, since nodes whose incoming edge is a Soft 5′ Splice Site cannot be included in the transcript unless the adjacent upstream node is also included. Similarly, a node whose outgoing edge is a Soft 3′SpliceSite requires the adjacent downstream node to be included. Given the six sets of simulated events of complexity K(n) (where n = 1, …, 6), we used polyester (Frazee et al., 2015) (read length = 100, error rate = 0) to simulate RNA-seq reads from the simulated transcripts for each gene (see Methods S1 for extended details).

Combinatorial gene model

To investigate engineering *de novo* AS analysis capability for transcript-level methods, we utilized Whippet's CSGs (in the Whippet/bin/simulation/*whippet-combinatorial.jl* script) to enumerate combinatorial graph paths for each pair of TxStart and TxEnd boundaries. While we successfully simulated combinatorial paths for a sliding window of four, five, six, eight, and ten nodes, we used four nodes throughout the manuscript (referred to as the 'N4 annotation Gene Transfer Format [GTF]'). This was the largest number of nodes in a sliding window for which, due to memory usage issues, we were able to successfully build indices using transcript-level methods.

Benchmarking

All genomic and transcriptomic sequences, as well as GTF files, were downloaded from the Ensembl database. The following genome builds were used: Hg19 GRCh37.p12 (v73) and Mm10 GRCm38.p4 (v84) using the full Ensembl GRCh37.73 annotations for all programs unless otherwise stated in the analysis or in the online instruction manual for that program (e.g., Figure 2A uses the full Ensembl annotation sets by default, while Figure 2B restricts each program to GENCODE v25 TSL1 or RefSeq Release 84 as specifically stated; see Table S4). Exon annotations (including genomic annotations) were downloaded from Ensembl using BioMart.

All benchmarking was performed on a Sun Microsystem X4600M2 server with 8 AMD Dual-Core 8218 CPU @2.6GHz, total 16 cores and 64GB RAM. The local hard disk was SATA 73GB, 10K RPM. Identical paired-end HeLa data of increasing read-depths were employed for all resource usage benchmarking (see Table S3). All programs were run with default settings with additional settings described in Table S4. The default linux package "time" (/usr/bin/time – e.g., http://man7.org/linux/man-pages/man1/time.1.html) was used to measure the resource usage of each program. See Methods S1 for extended details, and Tables S2 and S5 for results.

Benchmarking of mapping success was performed using the program Benchmarker for Evaluating the Effectiveness of RNA-Seq Software (BEERS) (http://www.cbil.upenn.edu/BEERS/) and simulated reads based on hg19 GRCh37.73 Ensembl transcriptome data. Simulated reads were generated using "reads_simulator.pl" with substitution frequency (parameter "-subfreq") error rates of 0.001, 0.005 and 0.01, respectively and a read depth of 1,000,000. For resource and mapping benchmarks the program "time" was used (see above and Methods S1 for details, and Table S6 for results).

RT-PCR and RNA-seq data used in comparisons of Ψ values were generated from samples prepared from mouse cerebellum and liver tissue, as well as from stimulated and unstimulated human Jurkat T cell line cells (Vaquero-Garcia et al., 2016). $\Delta\Psi$ values were calculated by comparing Ψ values between the mouse cerebellum and liver tissues samples or between the stimulated and unstimulated human Jurkat T cells. Only simple events (as defined by MAJIQ as involving a total of three exon-exon junctions) were included in the analysis.

Tissue-wide analysis of splicing

Low-entropy AS events are defined by an entropy value less than 1.0. High entropy events (for description of entropy of AS events see Figure 2D, Figures S4C and S4D and Methods S1) are defined as events with an entropy score of greater than 1.5, and differential entropy requires a change of entropy of greater than 1.0 (unless stated). Highest entropy events are defined as those greater than 2.0. Only events with a Whippet confidence interval width of less than 0.2, and Ψ values of over 0.05 and under 0.95 were included in the analyses. Analyses were limited to core exons (CE), as defined by Whippet. An exception to this rule is when assessing the fraction of genes co-expressing two or more major isoforms. For this analysis, due to observation in Figure S6B, we used a minimum read cut-off of 20 in main text (see Figures 3B and S6C for additional cut-offs).

Tissue RNA-seq data analyzed in Figure 3 and Figure S6 were from the Illumina Bodymap2 dataset and supplemented with human tissue RNA-seq data from Kunming Institute of Zoology (Table S3). The maximum change in splicing entropy between tissues is the comparison of the lowest entropy of an exon/node compared to the highest entropy for the same exon/node between tissues. This is therefore not a measure of tissue-specificity but rather a measure of maximum variability for the number of well-expressed exon-exon junctions an exon may have across tissues.

The analysis of how many genes co-express at least two isoforms at similar levels was calculated using the above tissue specific data. For an event to be considered as co-expressed the two principal isoforms must be expressed at similar levels (within a 10% range). Expression was assessed based on assigned reads. All types of splicing events were considered.

Tissue-wide heatmaps were generated by affinity propagation clustering using the R package (apcluster) with pairwise similarities as correlations (corSimMat and r = 2) and negative correlations taken into account.

Feature analysis of high-entropy AS events

For all amino acid residues in a protein, a score for predicted intrinsic disorder is computed using IUPred (Dosztányi et al., 2005). Amino acid residues with a score larger than 0.4 were considered as disordered. For each coding exon the proportion of total residues that are predicted to be disordered was estimated. Domain data extracted from SMART database (Letunic et al., 2015).

MaxEntScan (Yeo and Burge, 2004) was used to estimate the strength of 3′ and 5′ splice sites. 5′ splice site strength was assessed using a sequence including 3nt of the exon and 6nt of the adjacent intron. 3′ splice site strength was assessed using a sequence including −20nt of the flanking intron and 3nt of the exon. Exonic splicing silencer or exonic splicing enhancer densities were extracted from motifs quantified in (Ke et al., 2011). To calculate exonic splicing enhancer and silencer densities, all motifs defined by Ke et al. were summed together and normalized by the number of exonic nucleotides.

Analysis of cancer data

Hepatocellular carcinoma (HCC) and control data were from a transcriptome profiling study undertaken by the University of Hong Kong (see Table S3). For Figure 7A, all events with sufficient reads (n > 10) across multiple samples (more than 2) that showed evidence of AS ($0.05 < \Psi < 0.95$) were included in the analysis. These criteria were used throughout Figure 7, with the exception of Figure 7B, when all exons required at least 2 reads to support identification. For Figure 7B, unannotated alternative exon-exon junctions were extracted from the Whippet '.jnc' file.

Differential complexity between control and tumor samples across 15 replicates described in Figure 7C was assessed. Only samples with a significant difference (Mann-Whitney U test $p < 0.01$) and a median entropy difference between control and tumor samples of at least 0.5 were considered differential. To identify differentially expressed genes, read counts for transcripts (calculated by Whippet) were combined and DESeq2 (adjusted p value < 0.05) was used. SRSF1 overexpression data (Anczuków et al., 2015) was analyzed by Whippet. Only events with high entropy (> 1.5) in either the control or overexpression study were included in the analysis. Events with detected aberrant splicing in Figure 7I are displayed in Figure 7C.

QUANTIFICATION AND STATISTICAL ANALYSIS

Contiguous splice graph index

The central data structure underlying the alignment and quantification capabilities of *Whippet* is the Contiguous Splice Graph (CSG). This directed acyclic (i.e., except when circular splicing detection is enabled) graph structure is composed of all non-overlapping exon intervals, which are each defined as separate 'nodes'. Nodes in the CSG are connected by edges, defined as either splice junctions or adjacent exonic regions. All nodes are arranged consecutively in a single sequence based on genomic coordinates (see Algorithm S1 in Methods S1). As such, a CSG sequence built from a set of annotated transcripts may not necessarily resemble any of the individual transcript sequences. Each transcript sequence can however be defined by a sequential series of nodes through the graph. Whippet defines node boundaries (one upstream and one downstream, flanking either side of the node sequence) to describe the incoming and outgoing connectivity to other nodes. Whether an edge can exist between two nodes is defined by their incoming and outgoing 'boundary-types'. Node boundary-types are formally made up of two properties: a classification and an alignment property. The classification property can be a transcription start (TxStart), transcription end (TxEnd), donor splice site (5′SpliceSite), or acceptor splice site (3′SpliceSite) (Figure S1B and Table S7). The alignment property is one of two categories: 'Soft' or 'Hard'. Soft boundaries are node boundaries adjacent to other nodes in the genomic sequence. For example, in Figure 1B, nodes 3 and 4 have Soft outgoing and incoming edges, respectively. This is because in an annotated transcript they are part of the same exon (i.e., zero

nucleotides exist between the end position of node 3 and the start position of node 4 in the genomic sequence). In contrast, Hard boundaries exist when one or more genomic nucleotides separate the nodes. For example, there is a Hard boundary between nodes 2 and 3 in Figure 1B because genomic sequence separates the nodes. The compatibility of two boundary-types is determined by three simple rules: (1) All outgoing 5′SpliceSite boundaries are compatible with all incoming 3′SpliceSite boundaries, (2) Soft boundaries are compatible with adjacent neighboring Soft boundaries, and (3) no Hard boundary is compatible with any other boundary except in the case of Rule #1 (Methods S1 for extended details). This distinction between CSG Hard and Soft boundaries allows boundary type-specific rules to be utilized for alignment extension. After building all CSGs, the CSG Sequences are concatenated into a single Multi-CSG sequence that is used to create a transcriptome Full-text index in Minute space (CSG FM-Index) (Ferragina et al., 2004) for full-text substring searches.

Whippet aligns RNA-seq reads to the CSG index by performing heuristic ungapped extensions from alignment seed sequences mapped to the CSG FM-Index (see Methods S1, Algorithm S2 for details). Using the CSG index, Whippet is able to efficiently align spliced reads to any combination of nodes in a CSG. To facilitate this, reads are aligned across spliced edges using nucleotide k-mers flanking annotated 5′ or 3′ splice-site node boundaries. Each 5′ or 3′ splice-site flanking k-mer indexes each of two global hash-tables (i.e., associative maps) that link to a list of (gene, node) tuples, respectively (Figure 1D). Spliced read alignment uses read k-mers at an alignment node boundary to match compatible nodes from the same gene (note all nodes with outgoing 5′ splice sites are compatible with all nodes with incoming 3′ splice sites) (Figure 1D, Figure S1; see Methods S1 for extended details). Read alignment in this manner affords considerable efficiency by storing minimal data while supporting *de novo* AS event identification.

AS event definition and PSI quantification

After all reads have been assigned full or partial (for multi-mapping reads) counts to the edges in a CSG (see Methods S1 for details of isoform-level quantification and multi-mapping read assignment), AS events are next built *de novo* to quantify AS. In order to define an AS event for a node, the set of edges connecting to – and skipping over the target node (*N*) – are collected, where the read count of a skipping edge must be $\geq$ 1% of the maximal connecting edge read count. The AS event built *de novo* for each node (referred to here as the 'target node' of the event) is initially defined by the span of the edges that directly connect or skip the target node. Whippet iteratively collects all edges that fall within the span of previously defined directly connecting or skipping edges (Figure 1E). Whippet then performs the same procedure for each non-target node within the AS event, extending the AS event as necessary to encompass all auxiliary edges, including edges for non-target nodes that do not directly skip or connect to the target node (Figure 1E). The set of paths through the AS event are then enumerated using Algorithm S3 (see Methods S1).

In order to quantify the AS event paths $i \in I$, we utilize the set of edges E in the event and the read count c_e assigned to each edge $e \in E$. Counts for each unique edge e that exist in only one path i are assigned fully. However, non-unique edges found in multiple paths have counts initially divided among their compatible paths with uniform probability, and then the maximum likelihood for the relative expression of each AS event path is estimated using the expectation-maximization (EM) algorithm. We define a compatibility matrix $\mathbf{y}_{e,i} = 1$ for an edge e existing in a path i, and $\mathbf{y}_{e,i} = 0$ otherwise (Bray et al., 2016). We define the length of path i as proportional to the number of edges in the path such that: $j_i \propto \sum_{e \in E} \mathbf{y}_{e,i}$ (see Methods S1 for extended details). The probability α of observing reads from an AS event path i with relative expression level ψ_i is then defined by $\alpha(i) = \frac{\psi_i j_i}{\sum_{p \in I} \psi_p j_p}$. The following likelihood function is therefore iteratively optimized in the EM algorithm:

$$\mathscr{L}(\alpha) \propto \prod_{e \in E} \left(\sum_{i \in I} \mathbf{y}_{e,i} \frac{\alpha(i)}{j_i} \right)^{c_e}$$

In the M-step, the relative expression of each path (ψ_i) is given by:

$$\psi_i = \frac{\sum_{e \in E} \alpha(e,i) c_e}{j_i}$$

In the E-step, the probability α of observing reads from an edge e and path i are:

$$\alpha(e,i) = \frac{\mathbf{y}_{e,i}\, \psi_i}{\sum_{p \in I} \mathbf{y}_{e,p}\, \psi_p}$$

The percent-spliced-in Ψ of the node n is then calculated as the sum of the normalized relative expression of the paths containing the node $\{I_n \subset I\}$:

$$\Psi_n = \sum_{i \in I_n} \widehat{\psi}_i, \quad \text{where} \quad \widehat{\psi}_i = \frac{\psi_i}{\sum_{p \in I} \psi_p}$$

It's important to note that the this represents a generative model for RNA-seq count data, assuming that counts from each edge are drawn independently from a multinomial distribution. While this assumption will not always be satisfied (e.g., for reads that span

multiple edges), assuming independence among edges simplifies the problem space considerably and in turn does not adversely affect the accuracy of the quantifications.

Whippet_TPM

To calculate PSI values for Whippet nodes from the Transcript Per Million (TPM) values calculated by transcript-level analysis tools such as Kallisto/Salmon (Bray et al., 2016; Patro et al., 2017) (in the Whippet/bin/simulation/*whippet-quant-bytpm.jl* script, a.k.a 'Whippet_TPM'), we utilize the quantification concepts described for SUPPA (Trincado et al., 2018). Briefly, $\Psi_n = \frac{\sum_{i \in I_n} \tau_i}{\sum_{i \in I} \tau_i}$, where n is the node being quantified, I is the set of transcripts in the gene, I_n is the set of transcripts containing node n in the gene, and τ_i is the TPM of transcript i. To simplify this script, only nodes guaranteed to be quantified correctly are used, i.e., Whippet_TPM only quantifies nodes with 3′SpliceSite incoming and 5′SpliceSite outgoing boundary types.

Statistical analysis

Gene function enrichment analysis (Figures 3b and 4d) was performed using g:Profiler (with the python package: gprofiler; http://biit.cs.ut.ee/gprofiler), which uses a hypergeometric test with multiple hypothesis testing correction, as originally described by Benjamini and Hochberg. Mann-Whitney U non-parametric statistical tests were used for comparing distributions (R query: Wilcox.test < default parameters >) in Figures 4A, 6B, 6C, 7A, 7C, 7H and, Figure S7. An exception was in Figure 2A and Table S1 when analyzing repeated-measurements (e.g., in RT-PCR comparisons), in which case the Wilcoxon signed rank test was used (R query: Wilcox.test – signed = T). Kolmogorov–Smirnov (KS) tests were used in Figure S9. Fisher's exact test (R query: fisher.test) was used for comparing two nominal variables in a small population in Figure 7I and Figure S6. DESeq2 (Love et al., 2014) tested for differential gene expression using negative binomial generalized linear models with a multiple hypothesis testing correction, as originally described by Benjamini and Hochberg. The adjusted p value cut-off was 0.05. Heatmaps were generated using Affinity Propagation clustering with the R package ''apcluster.'' Clustering was based on either pairwise similarities of correlations (Pearson), or mutual pairwise similarities of data vectors, measured as the negative Euclidean distance. Correlations were assessed using Pearson Correlation Coefficient.

Additional resources

Further benchmarking and methods details are described in Methods S1. Protocol is available at http://github.com/timbitz/Whippet.jl.

DATA AND SOFTWARE AVAILABILITY

Whippet is implemented in the high-level, high-performance dynamic programming language Julia (julialang.org) and is freely available as open-source software under the MIT license (Git repository: http://github.com/timbitz/Whippet.jl). The analysis scripts and simulated data used in this study are available at http://figshare.com/articles/Whippet_analysis_scripts/5711683.